Composites Part A: Applied Science and Manufacturing, Volume 37, Issue 11, November 2006, Pages 1983-2001.

Manuscript Draft

Manuscript Number: JCOMA-05-389R1

Title: Modelling damage and failure in carbon/epoxy Non Crimp Fabric composites including effects of fabric pre-shear

Article Type: Research Paper

Section/Category:

Keywords:

Corresponding Author: Prof. Anthony Pickett, PhD

Corresponding Author's Institution: Cranfield University

First Author: Lars Greve, PhD

Order of Authors: Lars Greve, PhD; Anthony K Pickett, PhD

Manuscript Region of Origin:

Abstract: A numerical material model for intra-laminar failure prediction of biaxial Non Crimp Fabric composites is presented. The model combines the elasto-plastic continuum damage constitutive model proposed by Ladevèze with the intra-laminar matrix failure model of Puck, and improves the shear damage representation using an exponential damage function. The work focuses on numerical model development for damage and failure prediction and validation for both unsheared and sheared fabric composites which will result from draping of the fabric preform over a double curved geometry in order to manufacture complex shaped parts. An extensive test program has been conducted using flat composite coupons with differing degrees of fabric pre-shear in order to establish a database of material stiffness, strength, and in-plane matrix shear damage evolution prior to failure. This database is used to identify parameters for the proposed 'Ladevèze-Puck' damage and failure model. Final validation has been made by implementing the model in

an explicit Finite Element code and performing a series of experimental and simulation analyses on transversely loaded circular composite discs having differing degrees of fabric pre-shear.

Composites Part A: Applied Science and Manufacturing, Volume 37, Issue 11, November 2006, Pages 1983-2001.

Paper: Composites Science and Technology

Modelling damage and failure in carbon/epoxy Non Crimp Fabric composites including effects of fabric pre-shear

L. Greve Volkswagen AG, Group Research, 38436 Wolfsburg, Germany

A. K. Pickett* School of Industrial and Manufacturing Science, Cranfield University, Bedford, MK43 0AL, United Kingdom

Abstract

A numerical material model for intra-laminar failure prediction of biaxial Non Crimp Fabric composites is presented. The model combines the elasto-plastic continuum damage constitutive model proposed by Ladevèze with the intra-laminar matrix failure model of Puck, and improves the shear damage representation using an exponential damage function. The work focuses on numerical model development for damage and failure prediction and validation for both unsheared and sheared fabric composites which will result from draping of the fabric preform over a double curved geometry in order to manufacture complex shaped parts. An extensive test program has been conducted using flat composite coupons with differing degrees of fabric pre-shear in order to establish a database of material stiffness, strength, and in-plane matrix shear damage evolution prior to failure. This database is used to identify parameters for the proposed 'Ladevèze-Puck' damage and failure model. Final validation has been made by implementing the model in an explicit Finite Element code and performing a series of experimental and simulation analyses on transversely loaded circular composite discs having differing degrees of fabric pre-shear.

Keywords

A. Polymer-matrix composites (PMC's)
B. Strength
C. Computational modelling
D. Mechanical testing

* Author for correspondence: Email a.k.pickett@cranfield.ac.uk

E. Nomenclature

Symbol	Description
$\{\boldsymbol{\sigma}\}$	Stress vector in the material co-ordinate system.
$\{\boldsymbol{\varepsilon}^e\}$	Elastic strain vector
$[\mathbf{C}]$, C_{ij}	Stiffness matrix and component.
ε_{ij}^e, ε_{ij}^p, ε_{ij}^t	Elastic, plastic, and total strain vector component.
E_{ij}^0, G_{ij}^0, υ_{ij}^0	Initial elastic modulus, shear modulus, and Poisson's ratio.
d_{ij}	Damage function.
Y_{ij}	Damage conjugate quantities.
b	Damage coupling coefficient.
$\overline{Y}$	Damage governing equation.
$\overline{Y}_{ij}^k$	Fitting parameters for damage functions.
W_e^0, W_e^d	Initial and damaged internal energy.
$\langle x \rangle_+$	Operator returning expression x if x is positive and 0 otherwise.
$sup_{\tau \le t}(x)$	Supremum of x: Maximum of x within the time frame $0 \le \tau \le t$.
G_{iC}	Critical strain energy release rate.

Symbol	Description
f	Yield function.
$\{\tilde{\sigma}\}$, $\tilde{\sigma}_{ij}$	Effective stress vector and component.
a	Anisotropy coefficient for yield function.
R_0, β, m	Yield stress, and hardening curve parameters (Ladevèze model).
$\varepsilon_{11,t}^{\max}$, $\varepsilon_{11,c}^{\max}$	Maximum fibre strain in tension and compression.
$\{\boldsymbol{\sigma}^{fail}\}$, σ_{ij}^{fail}	Matrix failure stress vector and component.
$\lambda_{Mode\ i}$	Mode dependent scaling distance to matrix failure envelope.
$R_\perp^{(+)}$, $R_\perp^{(-)}$, $R_{\perp\parallel}$	Basic strength in matrix transverse tension, transverse compression, and matrix shear direction.
$p_{\perp\parallel}^{(+)}$, $p_{\perp\parallel}^{(-)}$	Slope parameter of Puck fracture curve in transverse tension and transverse compression direction.
φ	Fibre orientation angle.
V_f	Fibre volume fraction.

1. Introduction

Advanced composites using Non Crimp Fabrics (NCF) and Liquid Composite Moulding (LCM) technologies are becoming increasingly attractive to the automotive (and other) industries for the economical manufacture of high performance parts in small series production runs. The absence of crimp gives high specific stiffness and strength, and biaxial NCF textile forms offer excellent drapeability for the manufacture of complex shapes. However, predictive failure models for these composites, suitable for impact and crash analysis, which can also account for fabric preshear, is required.

The potential intra-laminar failure modes of biaxial NCF are failure in one of the two fibre directions; either in tension or compression, and intra-laminar shear failure leading to fibre-matrix debonding. Lamina transverse matrix failure might also be observed; however, this mode will not initiate catastrophic ply failure since loading will be effectively transferred by the orthogonal tows of the adjacent plies. This is an observation recognised by Hart-Smith [1] in failure criteria he developed for

Unidirectional (UD) cross plies composites. A further possible composite failure mode is ply delamination; which has been investigated in a previous publication by the authors [16]. This failure mode is not considered here.

The excellent drapeability of NCF's allows both single and complex double curvature shapes to be formed, Figure 1. The shaping operation may cause extensive fabric shearing which will significantly modify local composite stiffness and strength properties. In excessively sheared areas fibre alignment will enhance strength in the fibre directions and render the composite vulnerable to failure under combined tension-shear loading in the transverse direction, Figure 1. For the work presented here a ±45° biaxial NCF having the specifications shown in Table 1 is used.

During the past three decades many composites failure models have been proposed and several have found their way into commercial Finite Element (FE) codes for prediction of ply failure. A recent comprehensive study to evaluate the most promising of these has been presented [2]. From this study the 'Puck' model [3] was highly rated and has been considered "*to be the best at capturing the qualitative characteristics of lamina and laminate behaviour*" [4]. However, it was noted that this theory neglected inelastic material deformations which led to significant underestimation of strains for matrix dominated load cases. A further noteworthy contribution to this study was by Cuntze [5] who, in many respects used a similar model to 'Puck' [6], but also accounted for matrix plasticity.

The constitutive model proposed by Ladevèze and Le Dantec [7] allows representation of matrix plasticity, combined with matrix damage; thus providing an improved basis for prediction of the stress-strain relation of the material. This paper presents a combination of the 'Ladevèze' model and the 'Puck' failure criteria to treat in-plane failure of carbon NCF reinforced composites under combined loading conditions; further improvements for representation of matrix shear damage development in NCF composites have also been necessary. The next section introduces the failure models, followed by sections on parameter identification and validation. Both unsheared and pre-sheared fabric composites have been considered in the experimental and numerical work. It is believed that the techniques presented are, in principle, also applicable to other biaxial textile reinforced composites such as conventional woven fabrics.

2. Material Modelling

2.1. The damage constitutive model

The classical continuum damage mechanics model proposed by Ladevèze and Le Dantec has been implemented in a multi-layered thin shell element in the explicit Finite Element code PAM-CRASH™

[8]. This allows each ply in the laminate to be represented using an orthotropic elasto-plastic, with damage, stress-strain relationship given by,

$$\{\boldsymbol{\sigma}\} = [\mathbf{C}]\{\boldsymbol{\varepsilon}^e\}. \tag{2-1}$$

The stress and strain vectors are,

$$\{\sigma\}^T = \{\sigma_{11} \quad \sigma_{22} \quad \sigma_{12} \quad \sigma_{23} \quad \sigma_{31}\}^T,$$

and

$$\{\boldsymbol{\varepsilon}^e\}^T = \{\varepsilon^e_{11} \quad \varepsilon^e_{22} \quad \varepsilon^e_{21} \quad \varepsilon^e_{23} \quad \varepsilon^e_{31}\}^T,$$

and the stiffness matrix [**C**] has the following form and coefficients,

$$[\mathbf{C}] = \begin{bmatrix} C^0_{11} & \upsilon^0_{21}C^0_{11} & 0 & 0 & 0 \\ \upsilon^0_{21}C^0_{11} & C^0_{22}(1-d_{22}) & 0 & 0 & 0 \\ 0 & 0 & G^0_{12}(1-d_{12}) & 0 & 0 \\ 0 & 0 & 0 & G^0_{23}(1-d_{12}) & 0 \\ 0 & 0 & 0 & 0 & G^0_{12}(1-d_{12}) \end{bmatrix}, \tag{2-2}$$

with

$$C^0_{11} = \frac{E^0_{11}}{1-\upsilon^0_{12}\upsilon^0_{21}} \quad ; \; C^0_{22} = \frac{E^0_{22}}{1-\upsilon^0_{12}\upsilon^0_{21}}.$$

In the above equations the material constants E^0_{11} and E^0_{22} are elastic modulii in the fibre and transverse directions, G^0_{ij} is shear modulus, and υ^0_{ij} is Poisson's ratio. The matrix dominated elastic modulii, $E_{22}{}^0$, $G_{12}{}^0$, and $G_{23}{}^0$, are modified by the damage functions (1-d_{ij}) during loading to failure. Two scalar damage functions d_{22} and d_{12} are introduced, having the range 0 (no damage) to 1.0 (fully damaged) to describe matrix damage development in the ply transverse and shear directions, respectively. Some simplifications for numerical implementation are made for out-of plane shear modulii. Based on the assumption of transverse isotropy, the shear modulus in the 1-2 and 1-3 directions are considered equal, $G_{13}{}^0 = G_{12}{}^0$. Consequently, equal damage development in both directions is assumed, $d_{13} = d_{12}$. For the sake of simplicity shear damage in the 2-3 direction is related to in-plane shear damage development, $d_{23} = d_{12}$. The theory assumes constant Poisson's ratio coefficients.

The damage functions (d_{22} and d_{12}) are associated with conjugate quantities Y_{22} and Y_{12}, which govern damage development. These quantities are partial derivatives of damaged elastic work with respect to the damage state and are analogous to the strain energy release rate G_{ic} used in classical Fracture Mechanics to describe strain energy released during crack growth [7]. The expressions for Y_{12} and Y_{22} are,

$$Y_{12} = \frac{\partial W^d_e}{\partial d_{12}} = \frac{\partial}{\partial d_{12}}\frac{1}{2}\{\boldsymbol{\varepsilon}^e\}^T[\mathbf{C}]\{\boldsymbol{\varepsilon}^e\} = \frac{1}{2}\left\{G^0_{12}\left[\left(\gamma^e_{12}\right)^2 + \left(\gamma^e_{13}\right)^2\right] + G^0_{23}\left(\gamma^e_{13}\right)^2\right\}, \tag{2-3}$$

$$Y_{22} = \frac{\partial W_e^d}{\partial d_{22}} = \frac{\partial}{\partial d_{22}} \frac{1}{2} \{\boldsymbol{\varepsilon}^e\}^T [\mathbf{C}] \{\boldsymbol{\varepsilon}^e\} = \frac{1}{2} C_{22}^0 \left(\left\langle \upsilon_{12}^0 \varepsilon_{11}^e + \varepsilon_{22}^e \right\rangle_+ \right)^2, \tag{2-4}$$

where the operator <...>+ distinguishes transverse tension and compression as follows,

$$\langle x \rangle_+ = \begin{cases} x & if\,(x > 0) \\ 0 & otherwise \end{cases}. \tag{2-5}$$

Damage development under matrix transverse compression loading is prohibited, equation (2-4), due to the assumption that existing matrix micro-cracks will close under compression loading, in which case the initial transverse elastic modulus is recovered. Damage interaction is introduced by the parameter b, leading to the final governing equation for coupled transverse-shear damage,

$$\overline{Y}(t) = \sup_{\tau \le t} \left(\sqrt{Y_{12}(\tau) + b Y_{22}(\tau)} \right). \tag{2-6}$$

Generally the coupling factor b is determined from experiments.

Enhancements to shear damage representation for NCF

A lamina under pure in-plane intra-laminar shear loading will exhibit matrix micro-cracks after a certain threshold stress is exceeded Figure 2a. These cracks will be normal to the direction of first principal stress and will extend until stopped by fibres crossing the crack paths. Continued loading will generate new parallel cracks, Figure 2b, until a saturated level of matrix micro-cracks is reached, Figure 2c. Further loading will cause micro-cracks to coalescence and form a macro-crack leading to material fracture Figure 2d. Based on these micro-mechanical considerations a corresponding macro-mechanical shear damaging law is proposed to approximate the real physical behaviour of the investigated NCF composite. An exponential shear damage function is used, in which the damage state asymptotically approaches the level of saturated damage, Figure 2e. Similar nonlinear shear damage development has also been observed and used for woven fabric pre-preg composites [9] and biaxial braid composites [10]. In the nonlinear shear damage function, Figure 2, $\overline{Y}_{12}^0$ represents the initiation of shear damage, $\overline{Y}_{12}^{fit}$ is a fitting parameter for the shape of the shear damage evolution curve, and d_{Sat} represents the saturation damage level.

Matrix plasticity

A cyclic tensile coupon test of a $[\pm 45]_{2s}$ laminate is used to characterise evolution of matrix shear damage and plasticity. The global laminate stresses and strains are transformed to assess the local ply shear stress-strain curve, Figure 3. The degradation of the ply shear modulus $G_{12,i}$ and the generation of inelastic ply deformation $\gamma_{12,i}^p$ can be clearly observed.

For NCF the plasticity model proposed by Ladevèze and Le Dantec for UD composites [7] has been found appropriate and is used here. Briefly, this is simple Von Mises yield criteria using an associated

flow rule to monitor the evolution of permanent plastic strains in the matrix caused by the transverse and shear strain components,

$$f = \sqrt{\tilde{\sigma}_{12}{}^2 + a^2 \tilde{\sigma}_{22}} - R(p) = 0\,, \tag{2-7}$$

with the effective stresses,

$$\tilde{\sigma}_{ij} = \frac{\sigma_{ij}}{1 - d_{ij}}\,. \tag{2-8}$$

Factor a^2 can account for material anisotropy. Assuming an isotropic matrix material it can be shown from the 'von Mises' yield condition that $a^2 = 1/3$.

A power law is assumed for plastic strain hardening,

$$R(p) = R_o + \beta p^m, \tag{2-9}$$

where R_0 is the shear yield stress, β and m are curve fitting parameters. The equivalent plastic strain p is given by,

$$p = \int (1 - d_{12}) d\gamma_{12}^p\,, \tag{2-10}$$

where the plastic shear strain increment $d\gamma_{12}^p$ is the difference between the total and elastic shear strain increments,

$$d\gamma_{12}^p = d\gamma_{12}^t - d\gamma_{12}^e\,. \tag{2-11}$$

Material parameter identification

The shear damage development and plastic hardening curve are determined by quasi-static cyclic tensile testing of $[\pm 45]_{2s}$ NCF composite coupons to failure, Figure 4. A rate of loading of 0.5 mm/min in an Instron 5500R-6025 testing machine has been used. The parameter identification for shear follows the procedures outlined in [7] with the new exponential shear damage function. Figure 5a,b shows the good fit of damage and hardening functions to experimental data points. For this work the exponential shear damage function has been implemented and used in a research version of the FE code PAMCRASH™.

The calibrated model parameters are summarised in Appendix I. Simulation of the cyclic tensile test using the new exponential damage function yields very good agreement with the experimental results, as shown by comparison of the longitudinal stress-strain curves in Figure 5c. Another simulation curve, computed using the original linear damaging function, is included for comparison. The linear damage approach leads to higher stresses at the beginning due to the underestimation of the damage state, Figure 5a. Furthermore, premature specimen failure is observed in this simulation once damaging localises and approaches the limiting value 1.0.

The original 'Ladevèze' model allows coupling of transverse tension damage and shear damage; $b \neq 0$ in equation (2-6). However, since carbon/epoxy biaxial NCF composites exhibit brittle elastic transverse tensile failure without significant damaging it is assumed that transverse deformation does not contribute to shear damage development; thus shear damage development is solely governed by shear deformation; $b \to 0$.

2.2. The Intra-laminar failure model

Fibre dominated failure: The elastic lamina modulii in the fibre direction ($E_{11t,c}$) and the corresponding maximum elastic strains ($\varepsilon_{11t,c}^{\max}$) have been obtained using standard tension and compression tests of $[0/90]_{2s}$ NCF coupons according to ASTM standards [11] and [12], Figure 6. The material model parameters obtained from these tests are summarised in Appendix I.

Matrix dominated failure: The in-plane intra-laminar matrix failure envelope proposed by Puck for a unidirectional lamina is represented by three different inter-connected curve functions, each representing a distinct failure mode A, B, and C, as shown in Figure 7.

The original 'Ladevèze' model contains a failure criterion for matrix failure which is directly related the to damage development [7]. As previously mentioned, only shear damage is assumed to be active occur under transverse compression loading, giving an open matrix failure envelope in the transverse compression direction, Figure 8. This is felt to be inappropriate for the NCF composite investigated here; although it is noted that recent work by Ladevèze et al. [13], has enhanced this failure mode to include transverse compression. In this work, however, the established 'Puck' failure criterion is preferred, so that matrix damage development and the matrix failure criterion are completely uncoupled.

For numerical integration of the Puck matrix failure criterion into an FE code it is convenient to use a scaling distance λ, defined as the ratio of the current stress vector $\{\boldsymbol{\sigma}\}$ to the extrapolated vector at the failure envelope $\{\boldsymbol{\sigma}^{\text{fail}}\}$, Figure 8, such that,

$$\{\boldsymbol{\sigma}\} = \lambda \{\boldsymbol{\sigma}^{fail}\}, \tag{2-12}$$

with

$$\lambda = \begin{cases} <1 & no\ failure \\ 1 & failure \\ >1 & post-failure \end{cases} \tag{2-13}$$

Based on the equations for matrix failure [14] the maximum λ for the different failure modes follows as,

$$\lambda = \begin{cases} \lambda_{ModeA} & if\left(\sigma_{22} \geq 0\right) \\ \lambda_{ModeB} & if\left(\sigma_{22} < 0 \quad and \quad 0 \leq \left|\frac{\sigma_{22}}{\sigma_{12}}\right| \leq \left|\frac{R_{\perp\perp}^{A}}{\sigma_{12c}}\right|\right) \\ \lambda_{ModeC} & if\left(\sigma_{22} < 0 \quad and \quad 0 \leq \left|\frac{\sigma_{12}}{\sigma_{22}}\right| \leq \left|\frac{R_{\perp\perp}^{A}}{\sigma_{12c}}\right|\right) \end{cases}. \tag{2-14}$$

With,

$$\lambda_{ModeA}(t) = \sup_{\tau \leq t}\left[\frac{p_{\perp\|}^{(+)} R_{\perp}^{(+)} \sigma_{22}(\tau) + \sqrt{\left(R_{\perp}^{(+)}\right)^2 \left(\sigma_{12}(\tau)\right)^2 + \left(\sigma_{22}(\tau)\right)^2 \left(R_{\perp\|} - p_{\perp\|}^{(+)} R_{\perp}^{(+)}\right)^2}}{R_{\perp\|} R_{\perp}^{(+)}}\right],$$

$$\lambda_{ModeB}(t) = \sup_{\tau \leq t}\left[\frac{p_{\perp\|}^{(-)} \sigma_{22}(\tau) + \sqrt{\left(\sigma_{12}(\tau)\right)^2 + \left(\sigma_{22}(\tau) p_{\perp\|}^{(-)}\right)^2}}{R_{\perp\|}}\right], \tag{2-15}$$

$$\lambda_{ModeC}(t) = \sup_{\tau \leq t}\left[\frac{-R_{\perp}^{(-)}\left(\sigma_{12}(\tau)\right)^2}{4\left(1 + p_{\perp}^{(-)}\right)^2 \left(R_{\perp\|}\right)^2 \sigma_{22}(\tau)} - \frac{\sigma_{22}(\tau)}{R_{\perp}^{(-)}}\right],$$

and,

$$R_{\perp\perp}^{A} = \frac{R_{\perp\|}}{2 p_{\perp\|}^{(-)}}\left(\sqrt{1 + 2 p_{\perp\|}^{(-)} \frac{R_{\perp}^{(-)}}{R_{\perp\|}}} - 1\right),$$

$$\sigma_{12c} = R_{\perp\|}\sqrt{1 + 2 p_{\perp\perp}^{(-)}}, \tag{2-16}$$

$$p_{\perp\perp}^{(-)} = p_{\perp\|}^{(-)} \frac{R_{\perp\perp}^{A}}{R_{\perp\|}}.$$

The material model parameters used in these formulae represent the material strength in pure loading directions, $R_{\perp}^{(-)}$, $R_{\perp}^{(+)}$, and $R_{\perp\|}$, and several curve fitting parameters, $p_{\perp\|}^{(+)}$, and $p_{\perp\|}^{(-)}$, representing the slopes of the fracture curve at $\sigma_{22} = 0$ in positive and negative transverse direction, respectively [14].

Calibration of the failure envelope for pre-sheared NCF

An investigation to assess failure of pre-sheared NCF composites under combined loading is undertaken. Testing coupons were manufactured from dry orthotropic biaxial NCF which were manually pre-sheared from ±45° to ±φ° and stacked in a sequence of $[\pm\varphi]_{2s}$ prior to Vacuum Assisted Resin Infusion (VARI). The coupons were then cut from the manufactured panels, providing different lay-up's ($[\pm\varphi]_{2s}$, $[\pm(90\text{-}\varphi)]_{2s}$, and $[0/2\varphi]_{2s}$) as indicated in Figure 9a. Two different pre-sheared composites were investigated; the first representing moderate fabric pre-shear (φ = 35°) and the second representing greater pre-shear (φ = 28°). The laminate thickness has been increased according to the amount of pre-shear in order to keep the fibre volume ratio approximately constant at V_f = 0.48 throughout the test programme.

Flat coupons were used for tension and compression testing using the procedures in [11] and [12] respectively, Figure 9b,c. All specimens were tested quasi-statically at 0.5 mm/min to failure in an Instron 5500R-6025 testing machine. The full testing programme undertaken is summarised in Figure 9d. Specimens tested in the fibre directions used monotonic loading to failure in tension and compression. The remaining specimens, $[\pm\varphi]_{2s}$ and $[\pm(90-\varphi)]_{2s}$, were tested using cyclic tension loading to failure in order to determine damage evolution and plasticity prior to failure. Table 1 summarises all results for fibre (tension and compression), and the cyclic shear failure cases.

Test results show an extensive nonlinear inelastic response for the $[\pm 28]_{2s}$ and $[\pm 35]_{2s}$ symmetric cyclic tension test coupons. Tension testing of the $[\pm 55]_{2s}$ and $[\pm 62]_{2s}$ coupons leads to a more linear elastic longitudinal stress-strain relation, according to an increased contribution of elastic transverse loading in these cases. Specimens loaded in the fibre direction, $[0/2\varphi]_{2s}$, generally exhibit brittle elastic failure under both tension and compression loading. For all these tensile tests it is noted that only minor experimental scatter is observed.

An inverse approach is used for the calibration of the matrix failure envelope. The procedure is visualised in Figure 10, and explained below.

The $[\pm\varphi]_{2s}$ and $[\pm(90-\varphi)]_{2s}$ tension tests are modelled using multi-layered shell Finite Elements in PAM-CRASH^{TM}, and simulated in order to determine the material model parameters for the matrix failure envelope. The simulations are stopped at the point of failure according to the maximum observed experimental longitudinal strain and stress traces (σ_{12} *versus*) of a ply element within the failure zone of each simulated test case are collected on to one chart, Figure 11. Within some simulations structural failure is initiated by fibre failure (denoted by square symbol in Figure 11). The remaining (circular) end points of the stress traces are used to 'fit' the 'Puck' failure envelope. Thus the puck failure envelope obtained is valid for all unsheared and pre-sheared NCF composites tested. The basic strength (σ_{22} for an individual ply) in transverse tension and compression direction cannot be determined from the biaxial NCF composite. Hence, these strengths have been estimated from tests on a unidirectional NCF having similar carbon/epoxy systems.

The material model parameters determined are summarised in Appendix I. For confirmation of this inverse material model parameter identification procedure, simulations of all test cases were repeated using the matrix failure model parameters identified. The computed stress-strain curves to failure are in good agreement with the experiments, Table 2.

3. Validation of Simulation Methodologies: Transversely Loaded Composite Discs

The previous section has outlined the test and material parameter identification procedures used to determine failure data for unsheared and pre-sheared NCF composites. This section describes a test that has been devised to validate the material models and material parameters.

The test involves circular composite discs of 120mm diameter which are simply supported on their perimeter and quasi-statically loaded transversely at their centre with a rigid hemispherical punch of 25mm or 50mm diameter. The discs rest on a slightly bevelled (15°) ring and are constrained by three concentric pins, Figure 12, to provide the simple support condition. The test setup was specially designed to realise rotational symmetry and minimise bearing effects on the boundary. The loading rate to failure was 0.5mm/min in an Instron 5500R-6025 testing machine. Different lay-ups, including unsheared and pre-sheared NCF, were used in this validation exercise.

Disc Manufacture and Testing: Flat panels of NCF composite were manufactured using the VARI process having lay-ups of $[0/90/\pm45]_s$, $[\pm45]_{2s}$, $[\pm38/\pm52]_s$, and $[\pm35]_{2s}$. The lay-up's $[\pm38/\pm52]_s$ and $[\pm35]_{2s}$ were generated by manually shearing ±45° biaxial fabrics. The circular discs were then cut from the finished panels and prepared for testing, Table 3. The punch force-displacement curves obtained from testing are summarised in Figure 13 and Figure 14.

All tests display a gradually increasing force until first structural failure. The 50mm diameter punch specimens tend to exhibit failure by a sudden crack developing between the punch and the outer rim of the disc, which leads to a rapid drop in force. The post failure force response displays significant residual strength after first structural failure since the large punch allows force redistribution away from the damage area beneath the punch. The smaller punch creates greater confined local damage as it penetrates the disc. Figure 15 shows typical final deformations of the composite discs after transverse loading by the large and the small punch. Only minor scatter is observed for tests using the larger punch, whereas more variation is found for the force-displacement curves of the smaller punch specimens. Most scatter is observed in the pre-sheared $[\pm38/\pm52]_s$ specimens.

Simulation of the Disc Tests: The composite discs have been modelled using an average element length beneath the punch of 4mm, Figure 16. The bevelled ring, including the pins and the punches, are all treated as rigid bodies. The punch is displacement driven in the transverse direction (normal to the disc) and standard contact definitions are applied between the composite disc, the punch and the ring.

The proposed combined 'Ladevèze-Puck' material model is used to represent the composite discs. The shell element used is a multilayered element in which the fibre orientation for each ply is defined

using material model parameters summarised in Appendix I. The experimental and predicted force-displacement curves are shown in Table 4, and computed contour plots of fibre and matrix damage are displayed in Table 5.

Discussion of Results: The simulation results of the discs can be divided into two principal structural failure types; namely, fibre dominated and matrix dominated failure. Fibre dominated structural failure is predicted for the $[0/90/\pm45]_s$, $[\pm45]_{2s}$ and, to a lesser extent, the $[\pm38/\pm52]_s$ discs; whereas matrix dominated failure is predicted for the $[\pm35]_{2s}$ discs. These predicted global failure modes are in good agreement with corresponding ultrasonic C-SCAN measurements of the tested discs, Figure 17.

Fibre dominated structural failure of $[0/90/\pm45]_s$, $[\pm45]_{2s}$ and $[\pm38/\pm52]_s$ discs: For the larger punch failure is indicated by sudden straight laminate cracks radiating between the disc centre and outer rim, whereas the smaller punch predicts localised disc penetration failure, Table 5. The predicted global failure patterns agree well with the experiments, previously shown in Figure 15. Furthermore, the predicted force-displacement curves for these tests are generally in good agreement with experimental results, Table 4.

Matrix dominated structural failure of $[\pm35]_{2s}$ discs: Matrix dominated structural failure is predicted for both punches, Table 5. In each case matrix damage originates beneath the punch and then gradually propagates toward the outer composite rim, structural failure occurs once the damage front approaches the bearing.

It is interesting to note that similar experimental force-displacement curves were obtained for both punch sizes for the $[\pm35]_{2s}$ discs. The predicted force-displacement curves for the $[\pm35]_{2s}$ discs exhibit earlier structural failure than the corresponding experiments. A likely reason is that mechanical failure data for intra-laminar matrix failure underestimates the true material strength. It has been observed experimentally that there is a size effect in that wider specimens provide greater strength and strain to failure. The cut face, especially for narrow coupons, provides a source of stress concentrations leading to premature failure; this condition is not representative of the semi-continuous material at the centre of the disc. Never-the-less, it is encouraging that this relatively simple and efficient Finite Element approach, using shell elements with average edge lengths suitable for large industrial FE analysis problems, can realistically predict failure for all the considered cases.

4. Conclusions

An experimental test programme using biaxial carbon/epoxy Non Crimp Fabric composites has been undertaken to establish a data set for matrix and fibre dominated damage and failure. Fabric pre-shear of biaxial NCF, potentially occurring during the preforming operation in complex shaped composite

parts, has to be addressed in failure analysis since fibre re-orientation renders the composite vulnerable to catastrophic combined matrix transverse-shear failure. Hence, the experimental test series has included the investigation of both unsheared and presheared biaxial NCF having differing degrees of fabric pre-shear. From this data a new failure law has been proposed that combines the elasto-plastic damaging constitutive model of Ladevèze and Le Dantec with the intra-laminar matrix failure model by Puck. Based on physical considerations, an exponential shear damage function has been established, which allows an improved representation of the shear damage development in these materials. All simulation methodologies have been implemented and tested using a research version of the PAMCRASH^{TM} code.

The 'Puck' matrix failure envelope was successfully calibrated to account for failure of unsheared and pre-sheared biaxial NCF composites. The combined 'Ladevèze-Puck' model has been validated using unsheared and pre-sheared NCF composite discs subject to quasi-static transverse loading. These tests generated a variety of global failure mechanisms, which could be well predicted by numerical simulation. Furthermore, the overall agreement of experimental and predicted punch force-displacement curves has been encouraging. It is felt that the proposed test and simulation procedures would also be applicable to other biaxial fabric composites such as woven fabrics.

References

[1] Hart-Smith LJ, "Predictions of the original and truncated maximum-strain failure models for certain fibrous composite laminates", Composites Science and Technology, 1998, 58(7), pp. 1151-1178.

[2] Harris B, Chou TW, Mai YW, Hinton MJ, Soden PD, Kaddour AS, "Failure criteria in fibre-reinforced polymer composites", Composites Science and Technology, Special Issue, Vol. 58, July 1998.

[3] Puck A, Schürmann H, "Failure analysis of FRP laminates by means of physically based phenomenological models", Composites Science and Technology, Volume 62, Issues 12-13, September-October 2002, pp. 1633-1662.

[4] Hinton MJ, Kaddour AS, Soden PD, "A comparison of the predictive capabilities of current failure theories for composite laminates, judged against experimental evidence", Composites Science and Technology, Vol. 62, Issues 12-13, September-October 2002, pp. 1725-1797.

[5] Cuntze RG, "The predictive capability of failure mode concept-based strength criteria for multi-directional laminates—part B", Composites Science and Technology, Vol. 64, Issues 3-4, 2004, pp. 487–516.

[6] Hinton MJ, Kaddour AS, Soden PD, "Recommendations for designers and researchers resulting from the world-wide failure exercise", Composites Science and Technology, Vol. 64, Issues 3-4, 2004, pp. 589–604.

[7] Ladevèze P, Le Dantec E, “Damage Modelling of the elementary ply for laminated composites”, Composites Science and Technology, Vol. 43, Issue 3, 1992, pp. 257-267.

[8] PAM-CRASH™ Users manuals, Engineering Systems International, 20 Rue Saarinen, Silic 270, 94578 Rungis-Cedex, France. www.esi-group.com

[9] Johnson AF, Pickett AK, Rozycki P, "Computational methods for predicting impact damage in composite structures", Composites Science and Technology, Vol. 61, Issue 15, 2001, pp. 2183-2192.

[10] Pickett AK, Fouinneteau MRC, “Material characterisation and calibration of a meso-mechanical damage model for braid reinforced composites”, Composites Science and Technology, In Press 2005.

[11] ASTM Standard (1995b), “Standard test method for tensile properties of polymer matrix composite materials”, D3039.

[12] ASTM Standard (1995a), “Standard test method for compressive properties of polymer matrix composite materials with unsupported gauge section by shear loading”, D3410/D3410M-94.

[13] Ladevèze P, Lubineau G, “On a damage meso-model for laminates: micro-mechanics basis and improvement”, Mechanics of Materials, 2002.

[14] Puck A, “Festigkeitsanalyse von Faser-Matrix-Laminaten : Modelle für die Praxis”, Hanser Verlag München Wien, 1996.

[15] Daniel IM, Ishai O, “Engineering mechanics of composite materials”, Oxford University Press, Inc., 1994, ISBN 0-19-507506-4.

[16] Greve L, Pickett AK, “Delamination testing and modelling for composite crash simulation”, Composites Science and Technology, 2005 [online available].

Figures

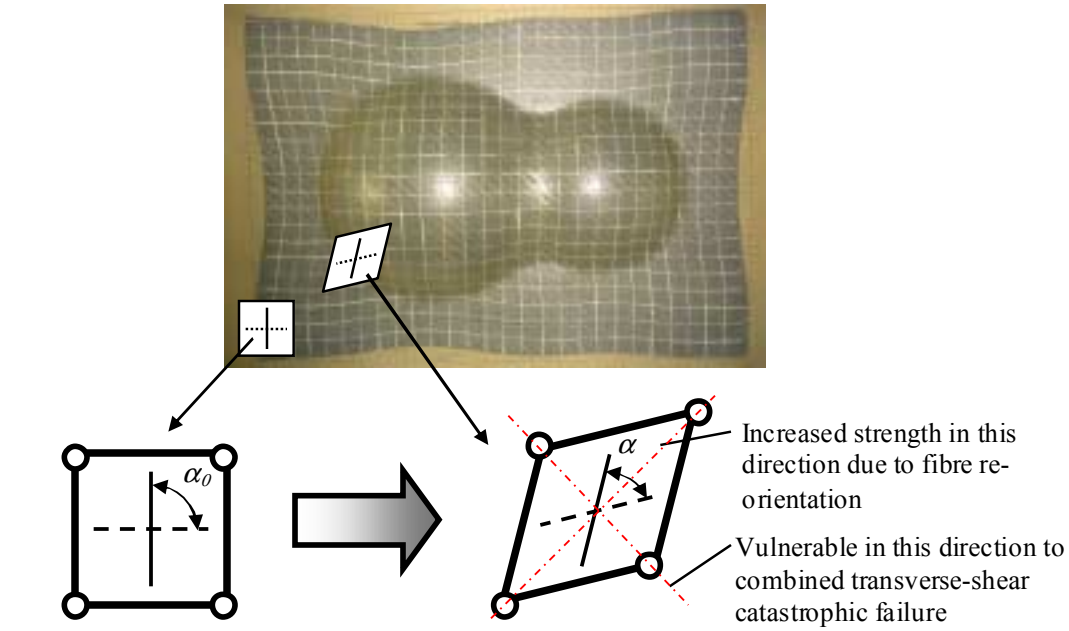

Figure 1. Fabric in-plane shear deformation of a biaxial (0/90) NCF due to draping over a double hemisphere surface.

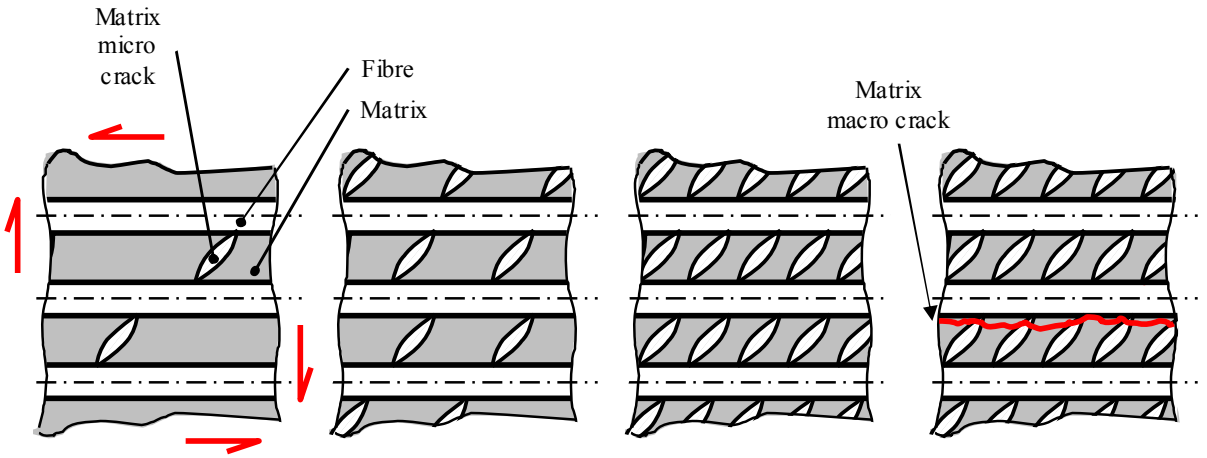

a) Initiation of matrix micro- shear cracking

b) Continuous matrix micro- shear cracking

c) Saturation of matrix micro-shear cracks

d) Formation of a macro- shear crack

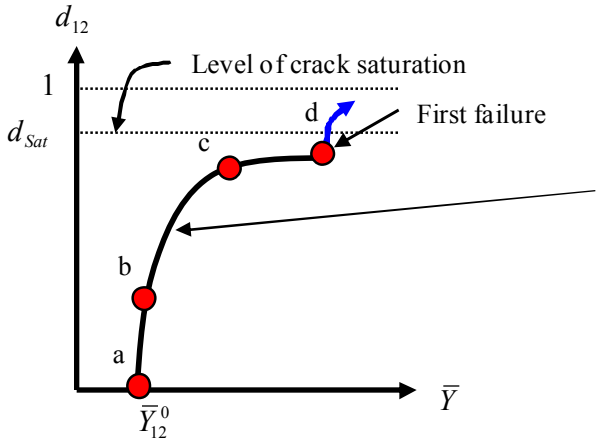

$$d_{12} = \begin{cases} d_{Sat}\left(1 - e^{\frac{\overline{Y}_{12}^{0} - \overline{Y}}{\overline{Y}_{12}^{fit}}}\right) & if\ \left(\overline{Y} > \overline{Y}_{12}^{0}\right) \\ 0 & otherwise \end{cases} \quad (4\text{-}1)$$

e) Macro-mechanical shear damage function for NCF representing the micro-mechanical failure phases (a-d)

Figure 2. Intra-laminar micro- and macro-crack formation under shear loading and corresponding shear damage function.

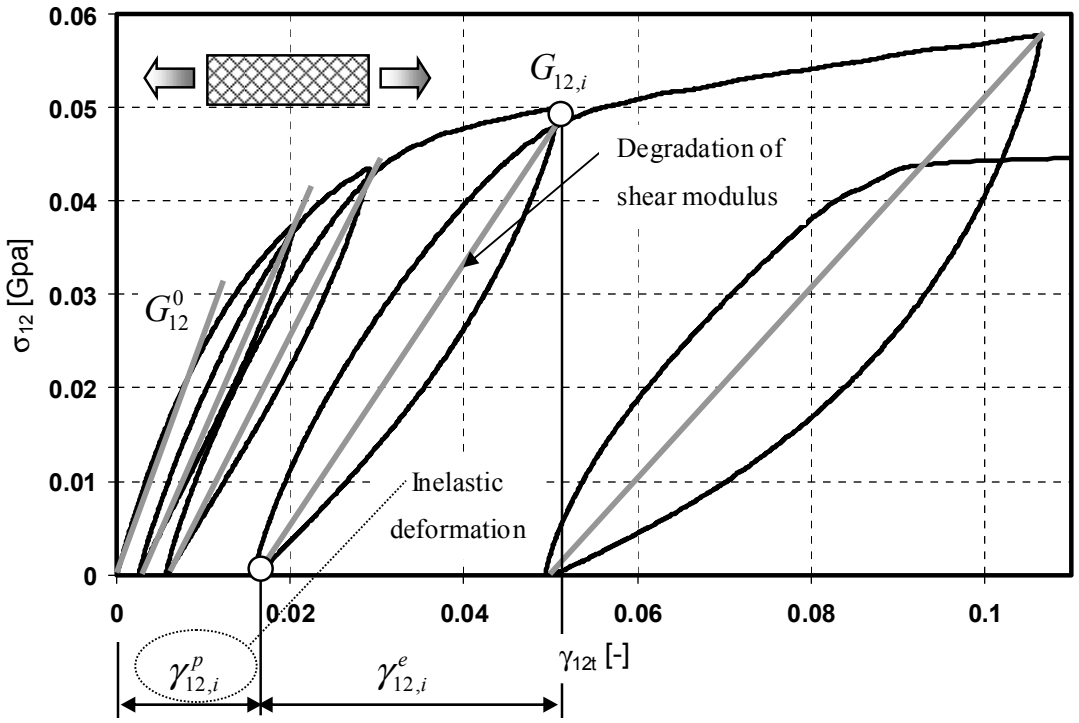

Figure 3. Lamina shear stress versus shear strain for a $[\pm 45]_{2s}$ cyclic tension coupon test.

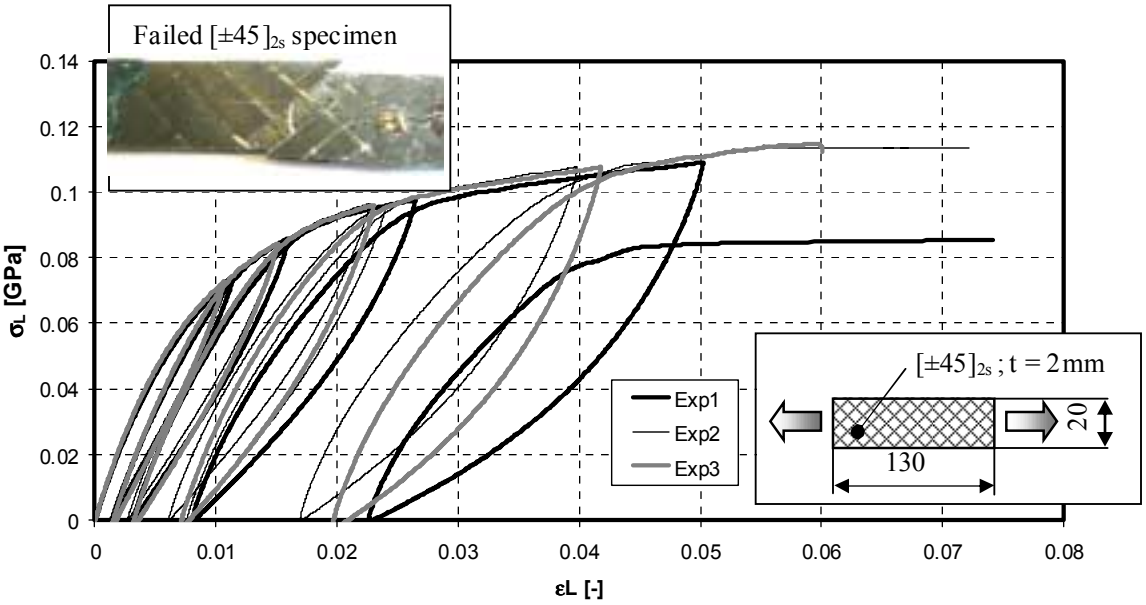

Figure 4. Longitudinal stress-strain curves for a cyclic tension $[\pm 45]_{2s}$ NCF coupon test.

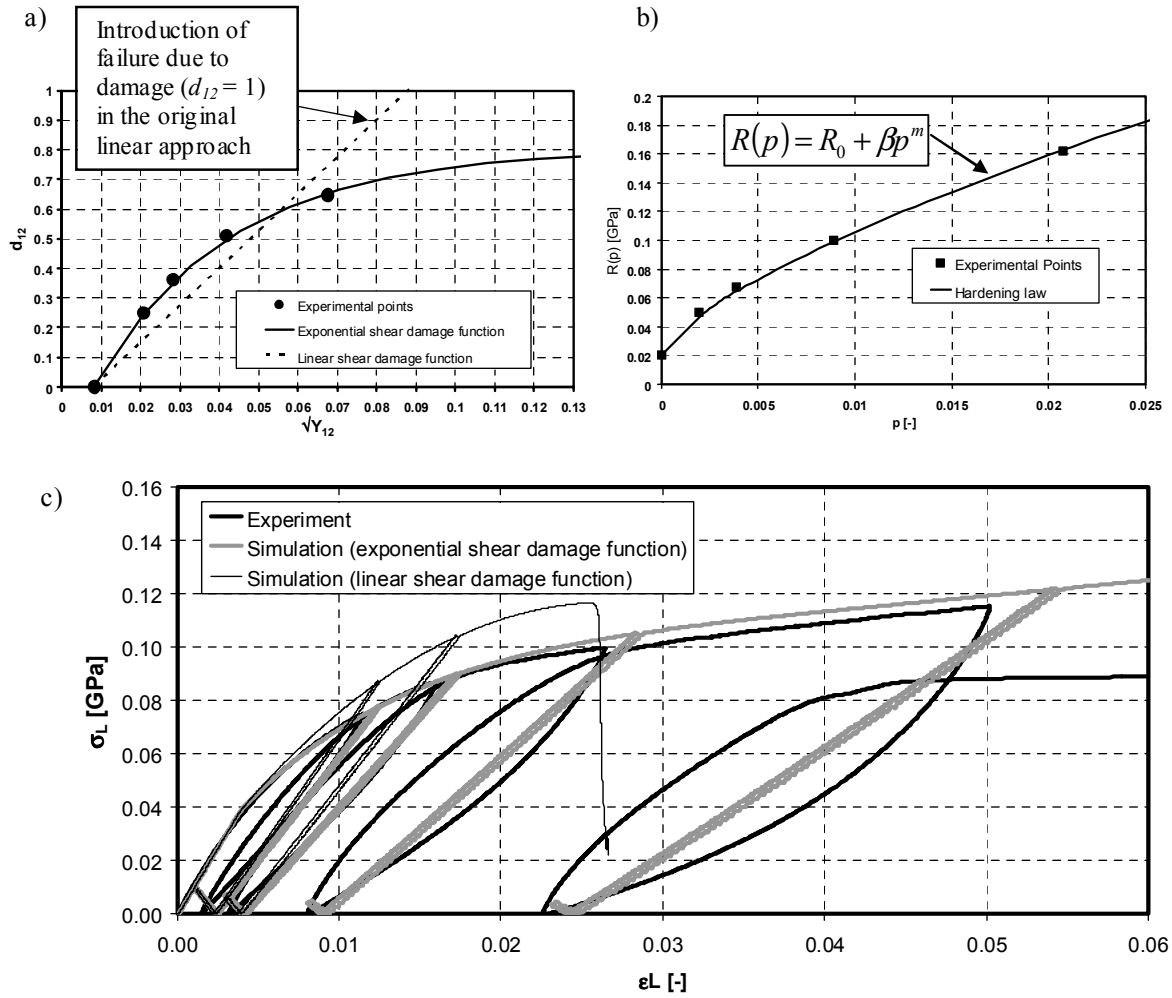

Figure 5. Calibration of the exponential shear damage function and plastic strain hardening curve:

a) Calibration of exponential and linear shear damage function

b) Calibration of plastic strain hardening function

c) Comparison of cyclic tension test and simulations using the original linear and new exponential damaging functions

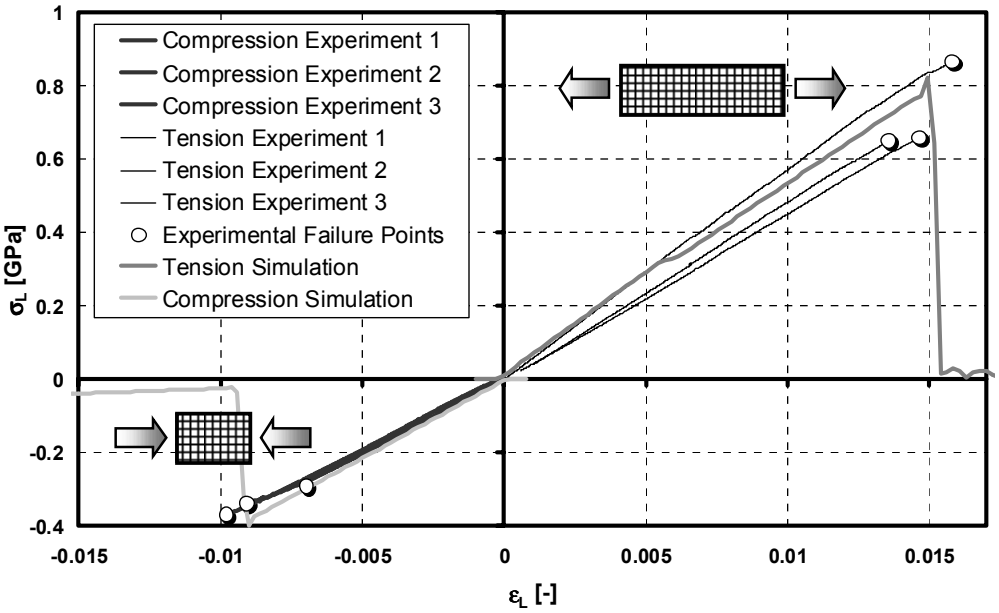

Figure 6. Tension and compression testing of $[0/90]_{2s}$ biaxial NCF coupons: Comparison of longitudinal stress-strain curves of experiments and simulations.

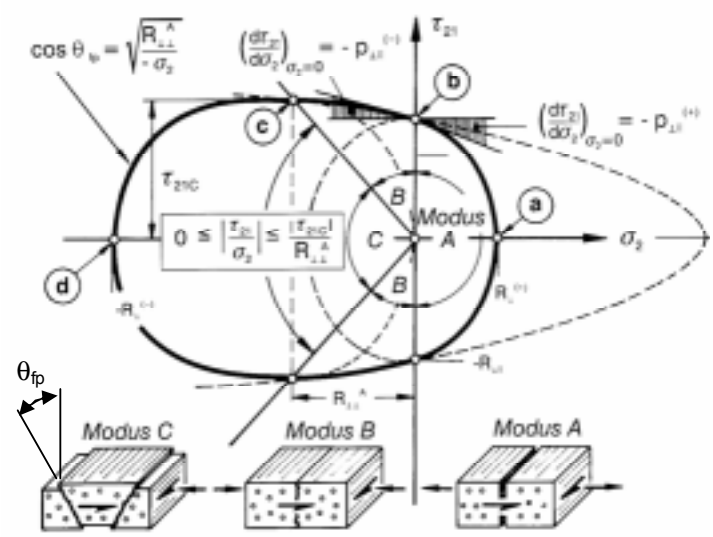

Figure 7. The 'Puck' matrix failure envelope in the in-plane matrix stress space [14].

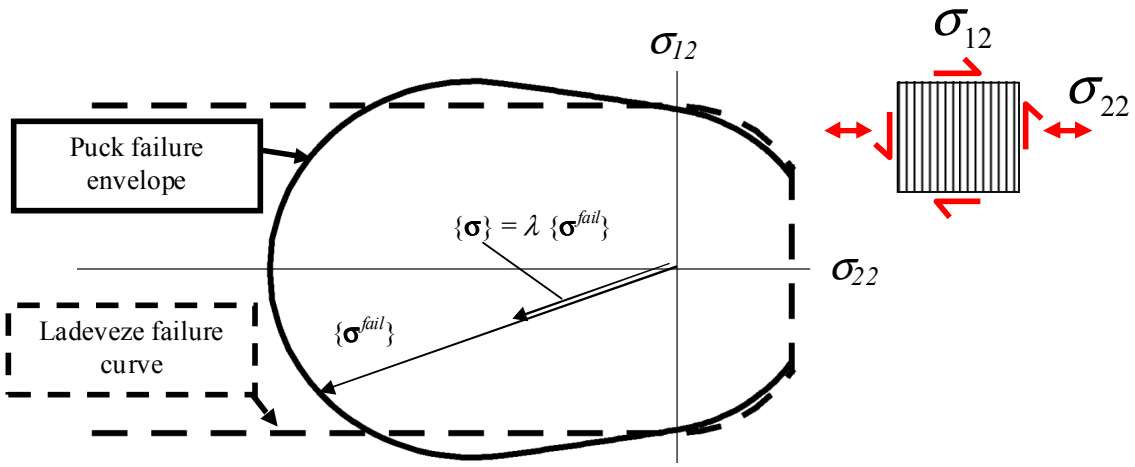

Figure 8. Principal comparison of the intra-laminar matrix failure curves proposed by Puck and Ladevèze.

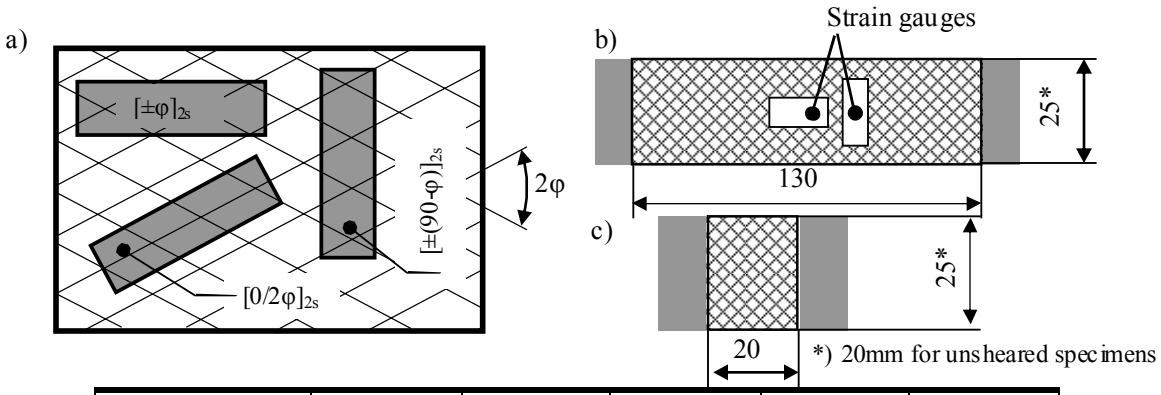

d)

Cyclic [±φ]2s tension	[±45]2s**	[±35]2s	[±28]2s	[±55]2s	[±62]2s
Sketch					
Thickness [mm]	2.0	2.1	2.6	2.1	2.6

**) Base fabric material (unsheared)

Simple [0/2φ]2s	[0/70]2s tension	[0/56]2s tension	[0/70]2s compr.	[0/56]2s compr.
Sketch				
Thickness [mm]	2.1	2.6	2.1	2.6

Figure 9. a) Specimen panels and cutting. b) Tension specimen dimensions. c) Compression specimen dimensions. d) Testing program of pre-sheared specimens.

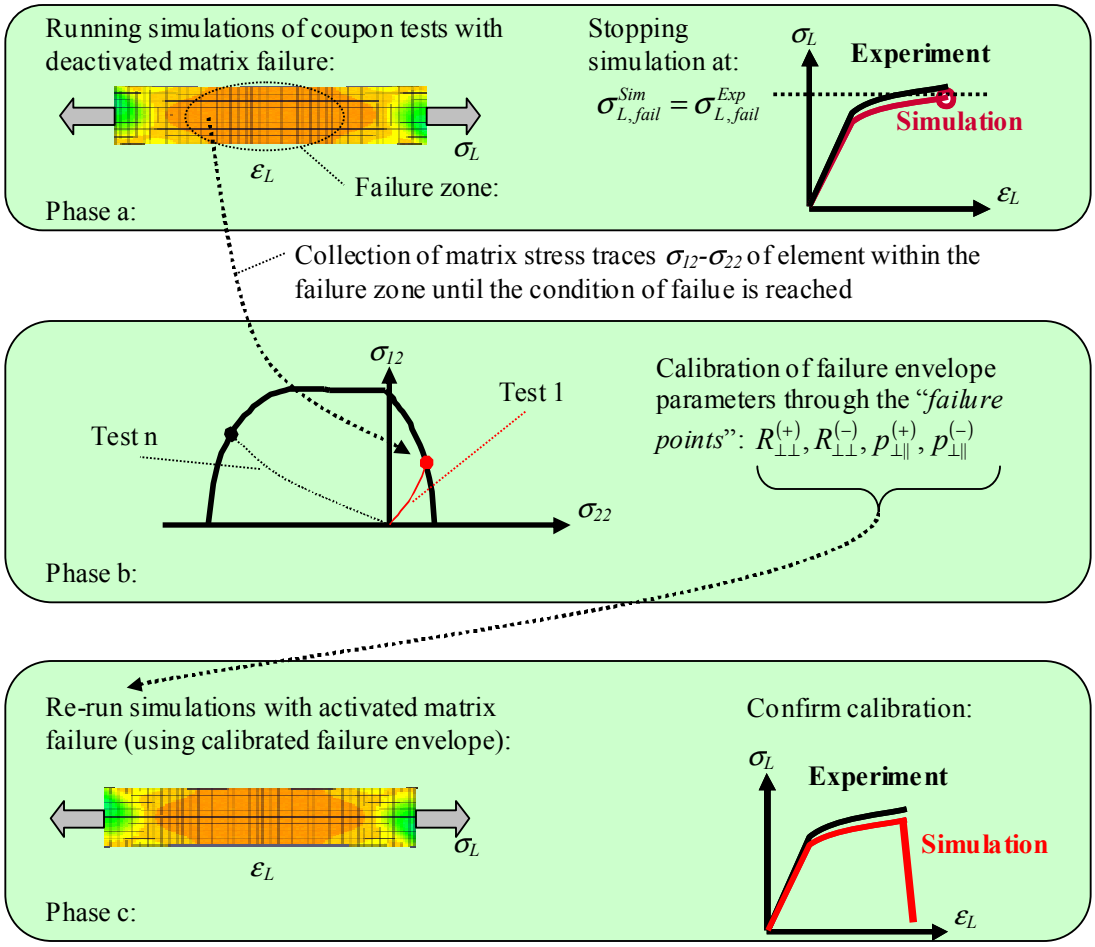

Figure 10. Procedure for the calibration of the matrix failure envelope using an inverse approach

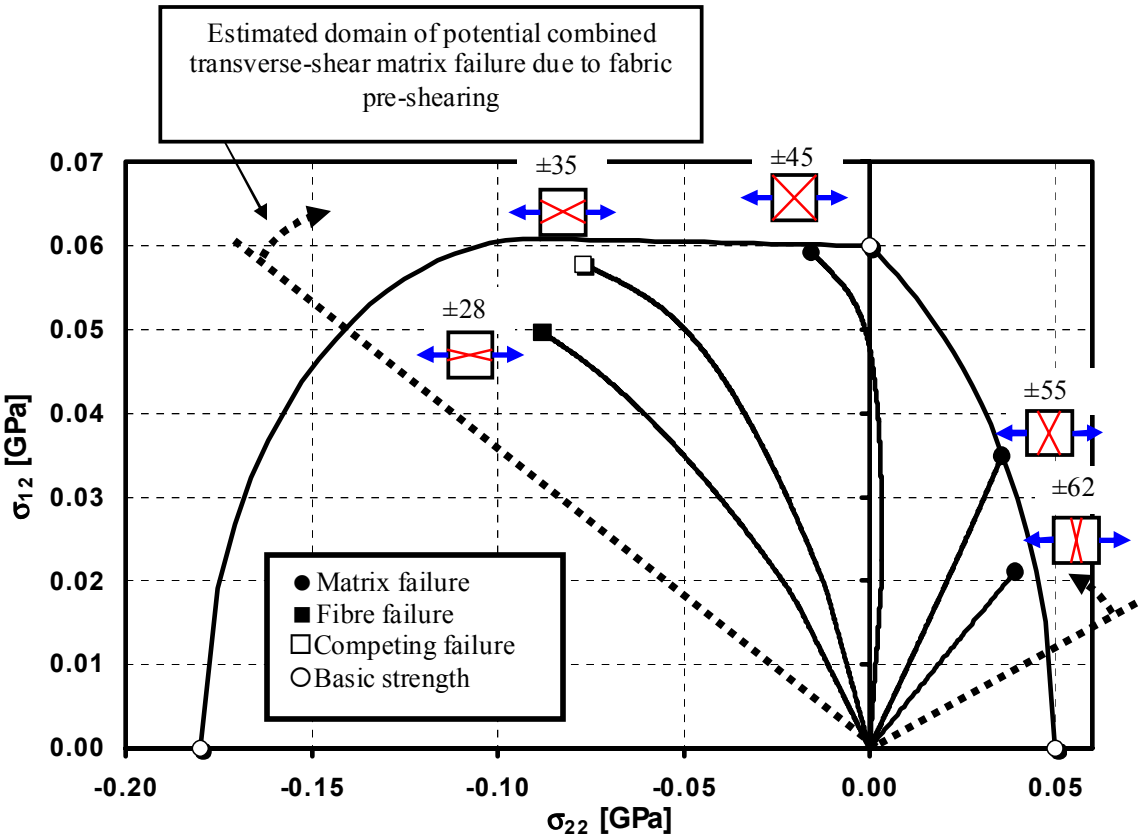

Figure 11. Stress traces of the $[\pm\varphi]_{2s}$ and $[\pm(90-\varphi)]_{2s}$ NCF coupons in the σ_{12}-σ_{22} space.

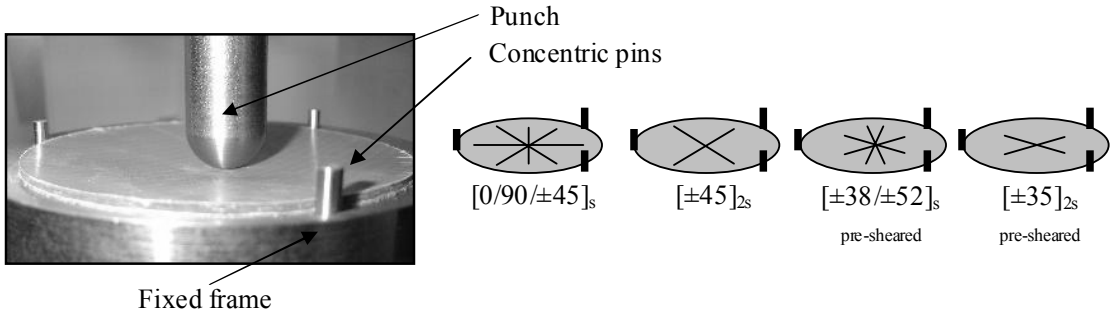

a) Test configuration and lay-ups

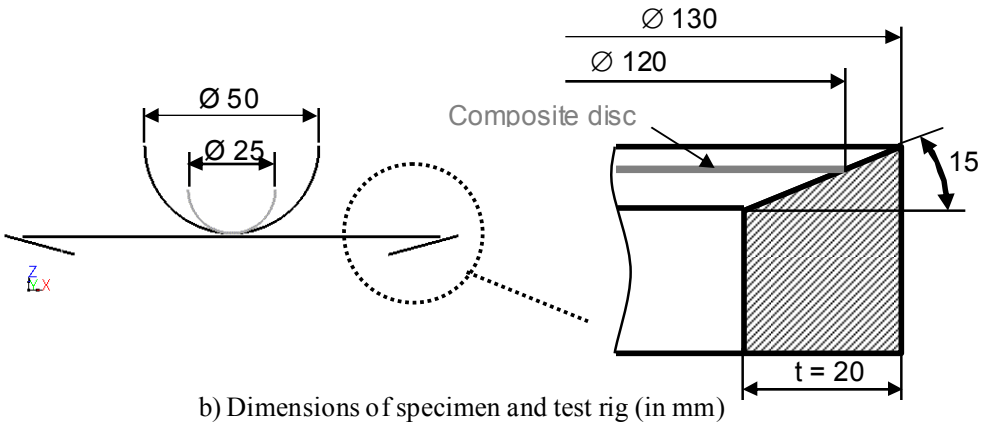

b) Dimensions of specimen and test rig (in mm)

Figure 12. Test configuration for the transversely loaded composite discs.

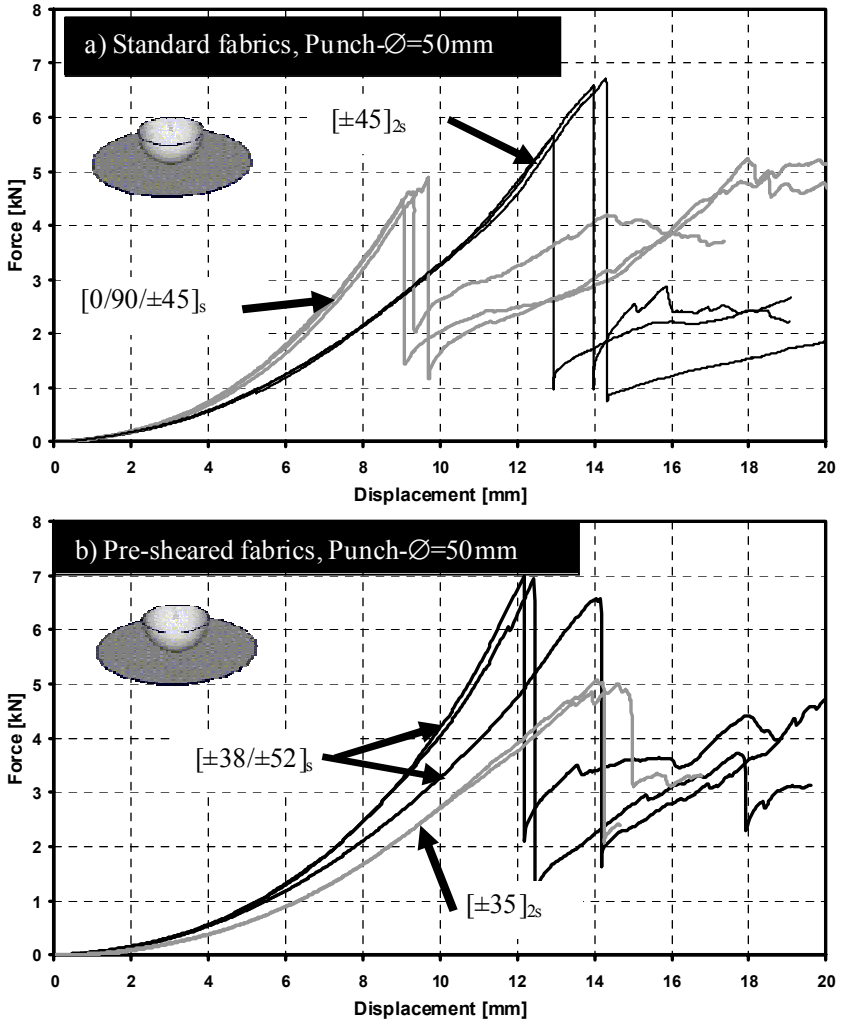

Figure 13. Experimental force-displacement curves for the composite discs subjected to quasi-static transverse loading to failure: Large punch (∅=50mm) results.

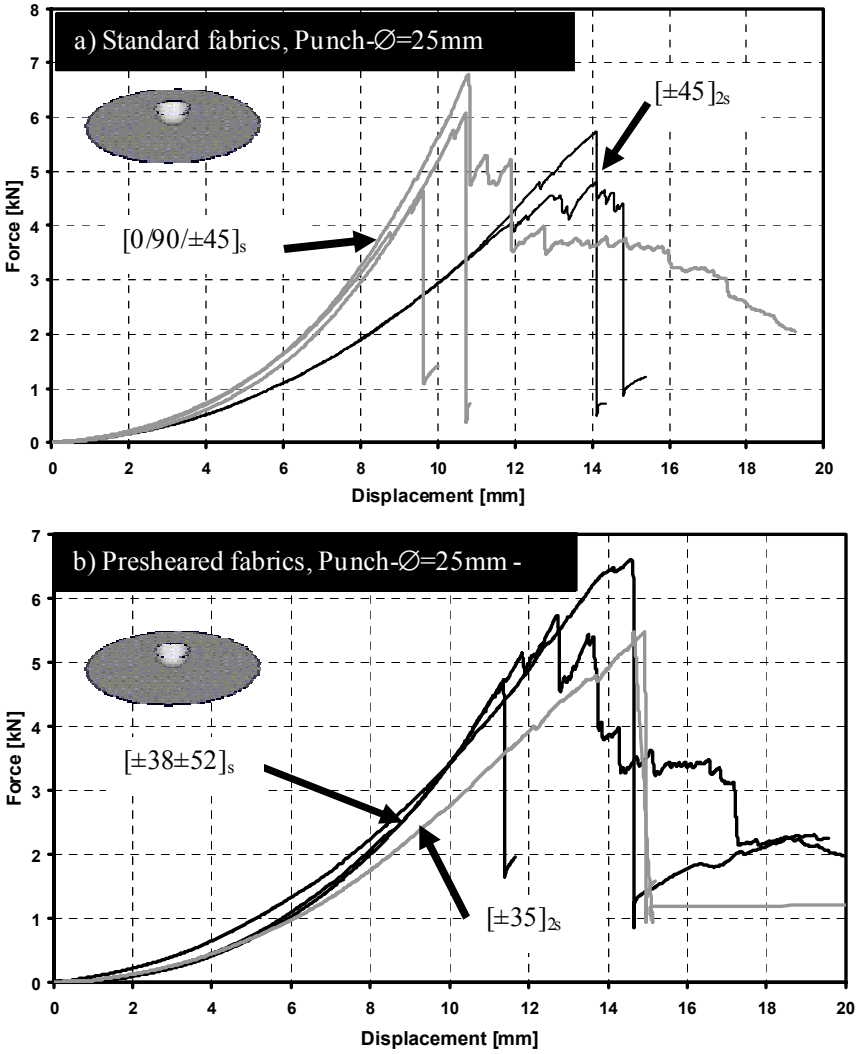

Figure 14. Experimental force-displacement curves for the composite discs subjected to quasi-static transverse loading to failure: Small punch (∅=25mm) results.

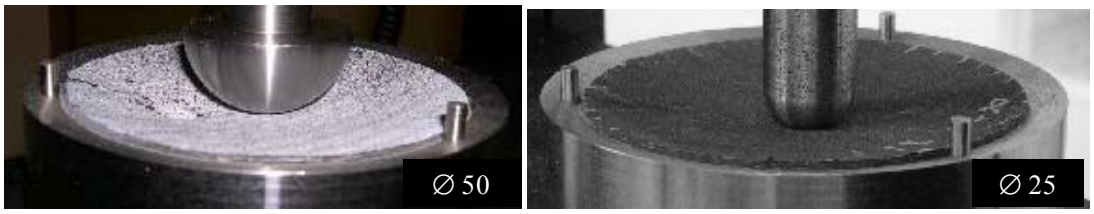

a) Failure deformations

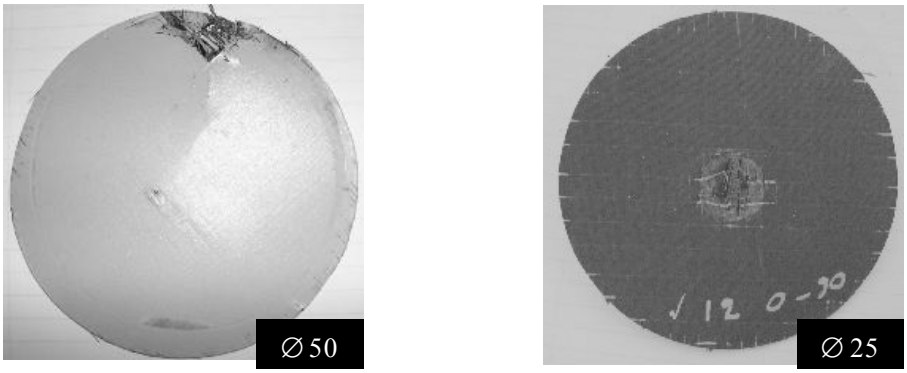

b) Final inelastic deformations (after spring-back)

Figure 15. Failure and final deformations of failed NCF composite disc specimens exemplarily shown for a $[0/90/\pm45]_s$ laminate.

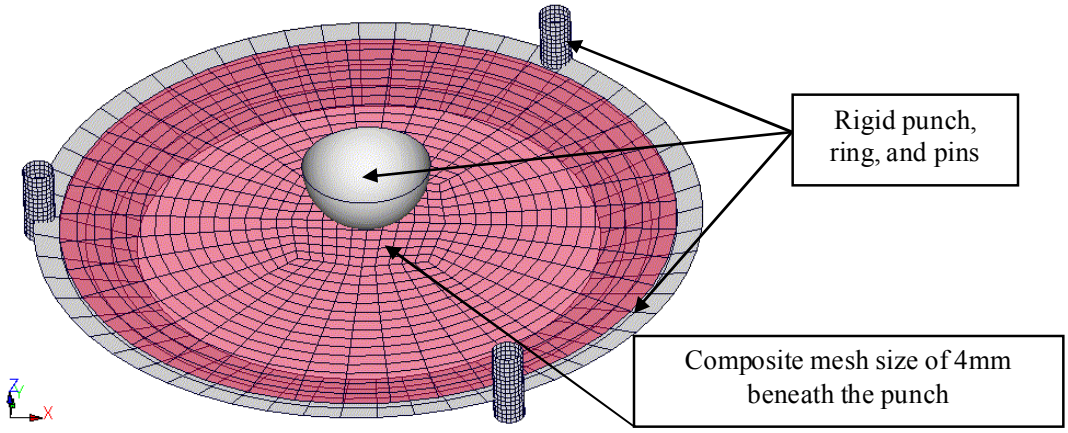

Figure 16. The setup and Finite Element model used for the transversely loaded NCF composite discs

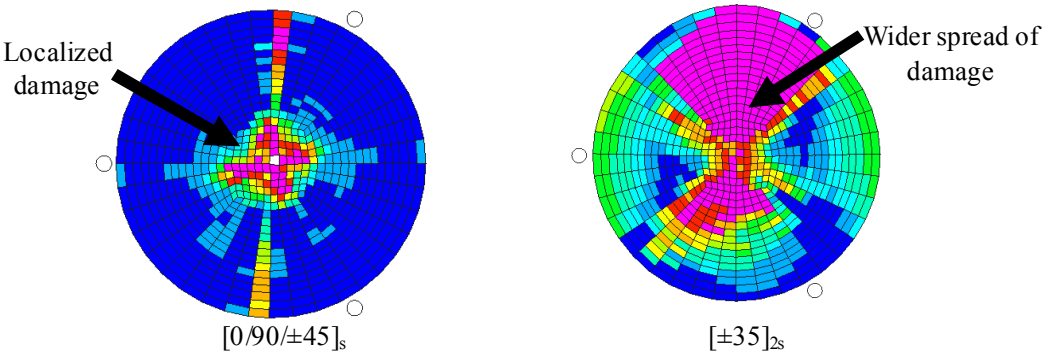

a) Qualitative comparison of computed average matrix damage development in a quasi-isotropic $[0/90/\pm45]_s$ NCF disc and a pre-sheared $[\pm35]_{2s}$ NCF disc transversely loaded using the large (∅50 mm) punch

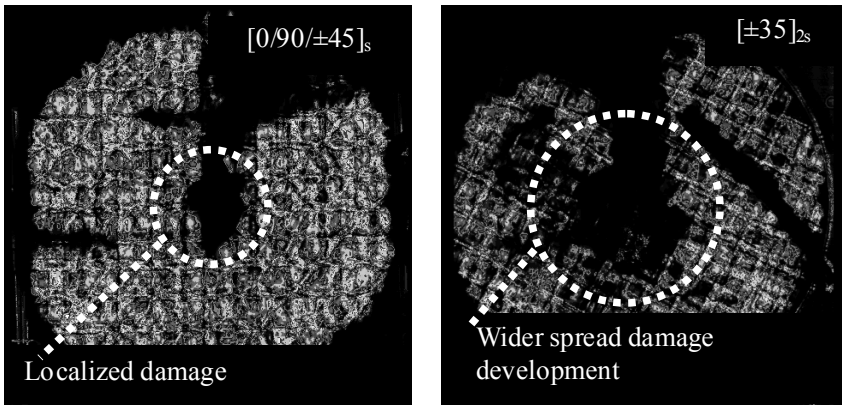

b) Ultrasonic C-Scans of the quasi-isotropic $[0/90/\pm45]_s$ NCF disc and the pre-sheared $[\pm35]_{2s}$ disc showing different degrees of internal damaging (dark regions) after transverse loading with the (∅=50 mm) punch

Figure 17. Comparison of computed matrix damage development and ultrasonic C-Scans for the NCF composite discs.

Tables

2-layer biaxial (±45) Non-Crimped Fabric	Specification
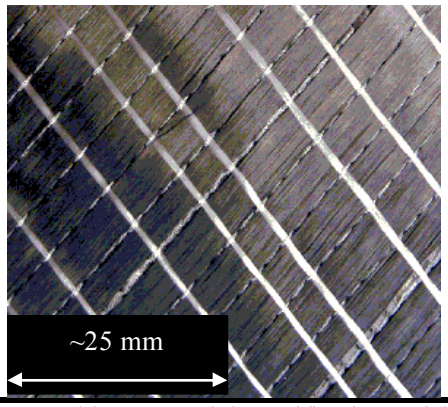	***Fabric Type:*** Biaxial 0/90 NCF fabric (m = 420 g/m²) 24k TORAY T600, carbon fibre Manufacturer: Saertex ***Epoxy System:*** LY 564 / HY2962 Fibre volume fraction: approx. 48 Vol.%

Table 4. Material specifications of the biaxial NCF carbon/epoxy composite material

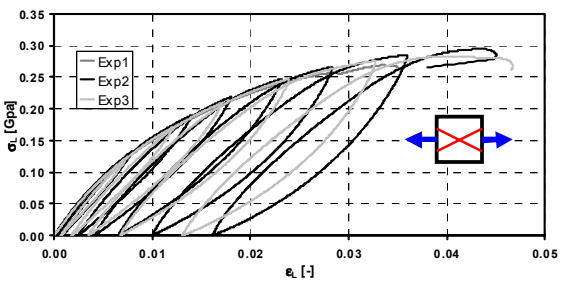

$[\pm 35]_{2s}$ cyclic tension

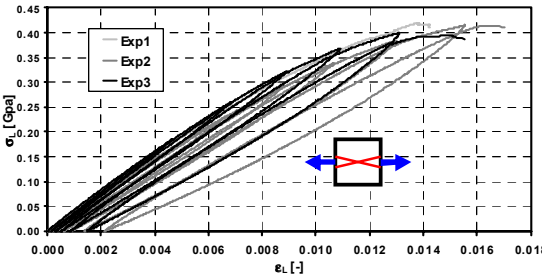

$[\pm 28]_{2s}$ cyclic tension

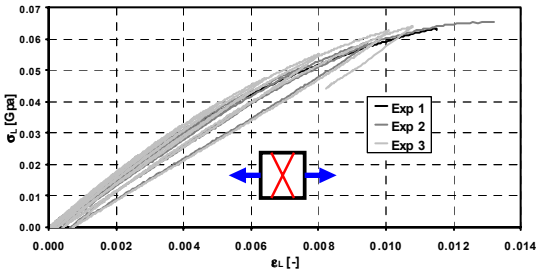

$[\pm 55]_{2s}$ cyclic tension

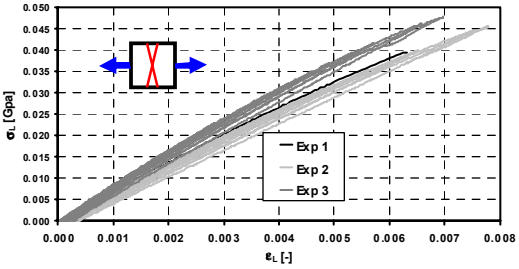

$[\pm 62]_{2s}$ cyclic tension

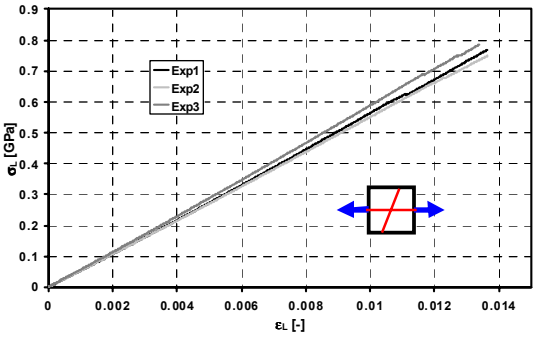

$[0/70]_{2s}$ tension

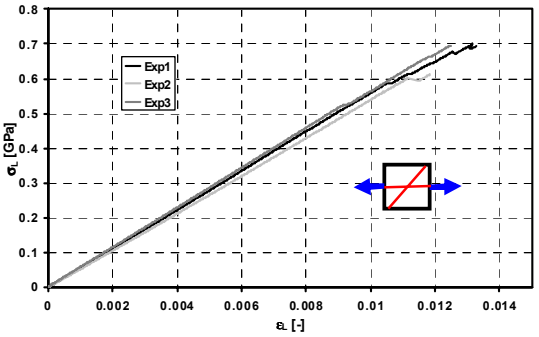

$[0/56]_{2s}$ tension

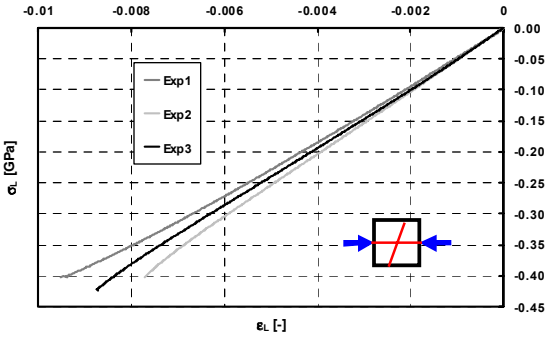

$[0/70]_{2s}$ compression

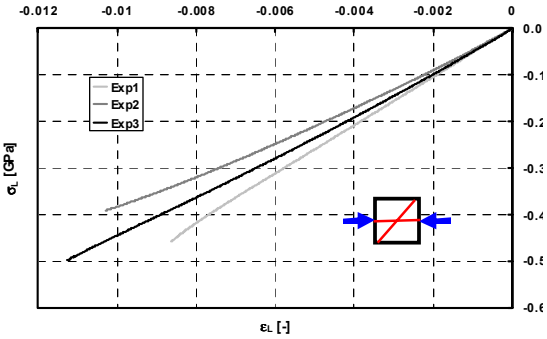

$[0/56]_{2s}$ compression

Table 1. Experimental longitudinal stress-strain curves for the pre-sheared NCF coupons.

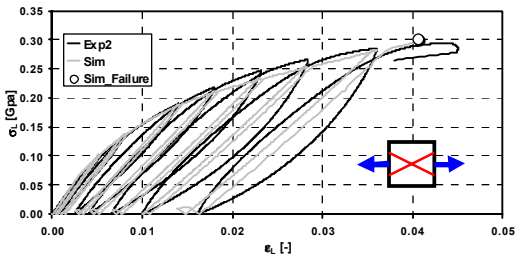

$[\pm 35]_{2s}$ cyclic tension

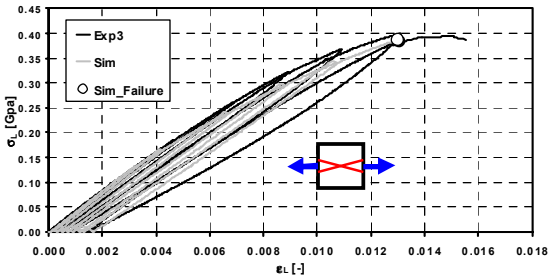

$[\pm 28]_{2s}$ cyclic tension

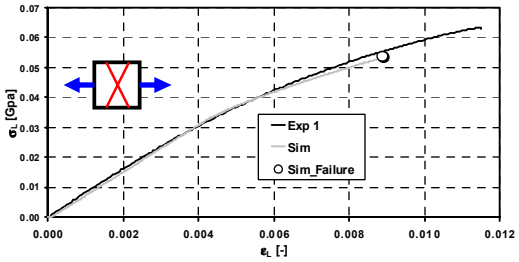

$[\pm 55]_{2s}$ cyclic tension

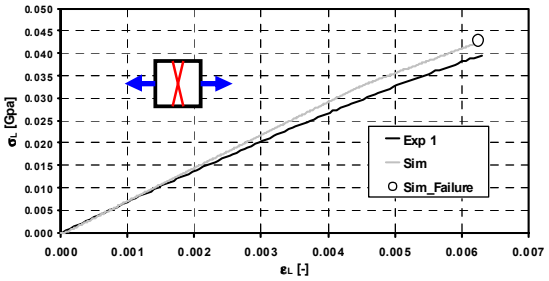

$[\pm 62]_{2s}$ cyclic tension

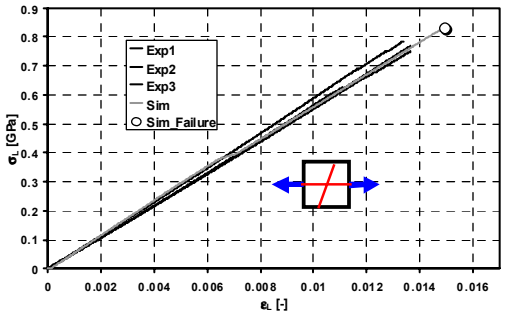

$[0/70]_{2s}$ tension

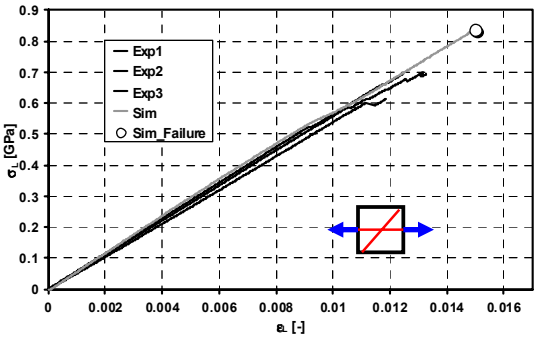

$[0/56]_{2s}$ tension

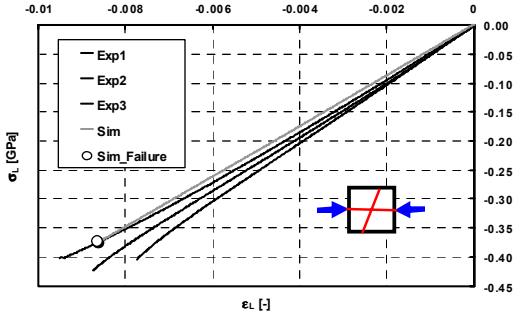

$[0/70]_{2s}$ compression

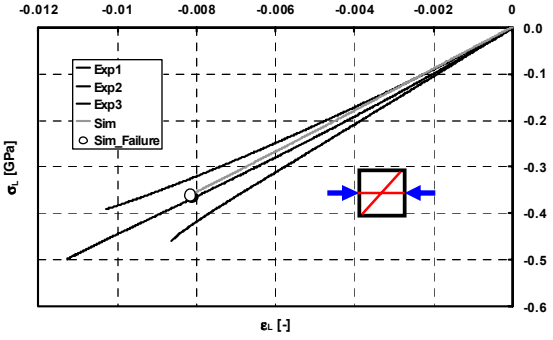

$[0/56]_{2s}$ compression

Table 2. Pre-sheared NCF coupons: Comparison of longitudinal stress-strain curves of experiments and simulations.

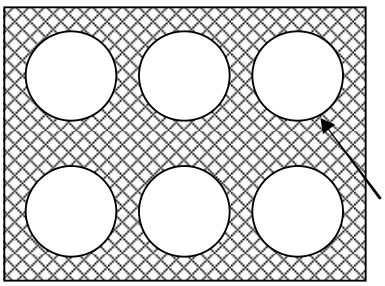

Disc extraction

Lay-up	Ø of punch [mm]	
	25	**50**
QI $[0/90/\pm45]_s$	3	3
$[\pm45]_{2s}$	2	3
$[\pm38/\pm52]_s$*	3	3
$[\pm35]_{2s}$*	2	2

*) Obtained from presheared ±45° NCF

Table 3. Test matrix for the transverse loaded composite discs using different lay-ups and punch diameters.

Lay -up	Small punch diameter (∅ = 25 mm)	Large punch diameter (∅ = 50 mm)
$[0/90/\pm45]_S$	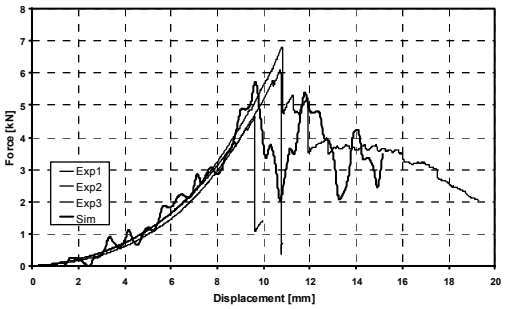	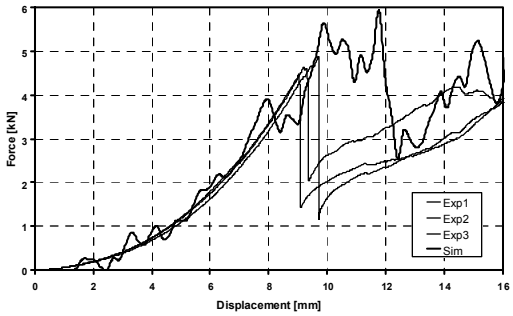
$[\pm45]_{2S}$	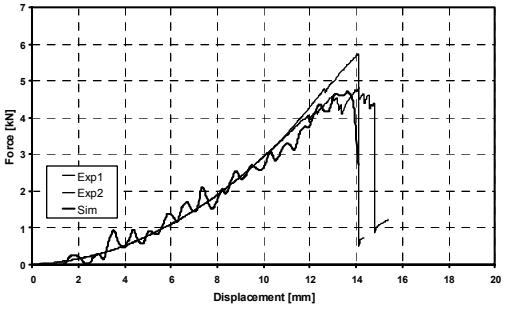	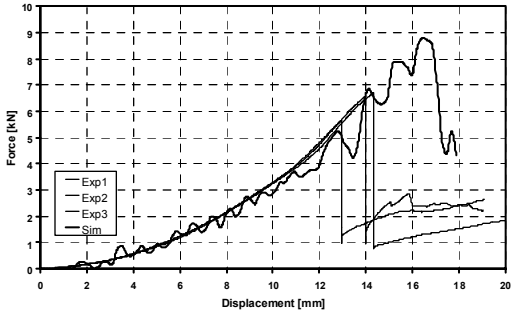
$[\pm35]_{2S}$	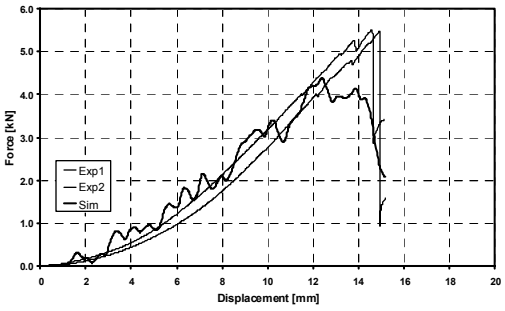	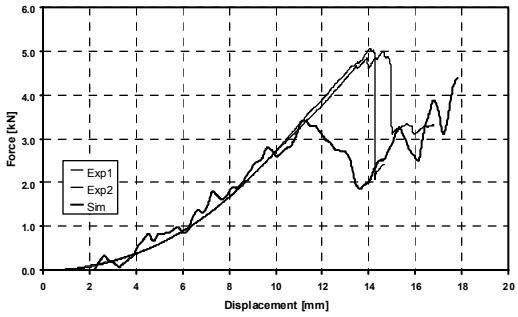
$[\pm38/\pm52]_S$	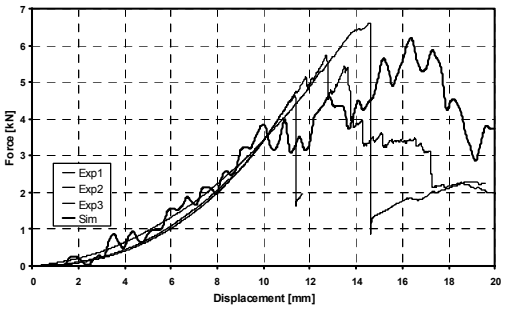	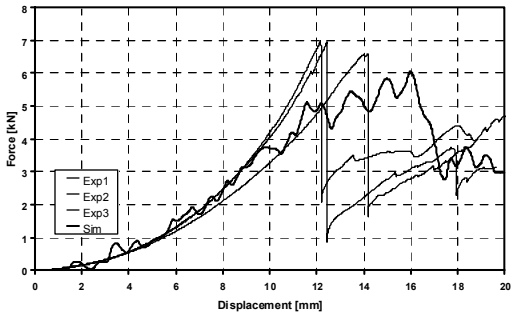

Table 4. Comparison of experimental and predicted force-displacement curves of transversely loaded NCF composite discs.

Lay-up	Small punch diameter (∅ = 25 mm)		Large punch diameter (∅ = 50 mm)	
	Fibre Failure	Matrix Failure	Fibre Failure	Matrix Failure
$[0/90/\pm45]_s$ 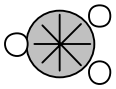	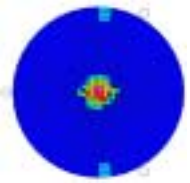	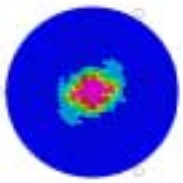	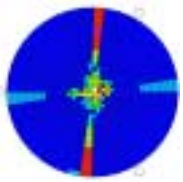	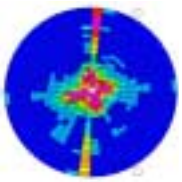
$[\pm45]_{2s}$ 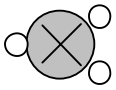	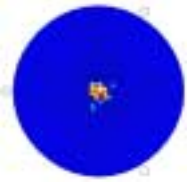	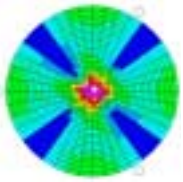	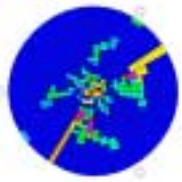	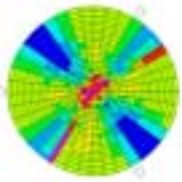
$[\pm35]_{2s}$ 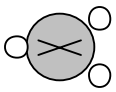	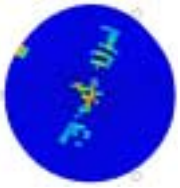	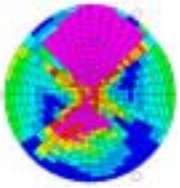		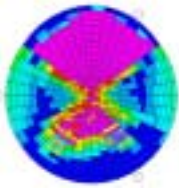
$[\pm38/\pm52]_s$ 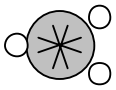	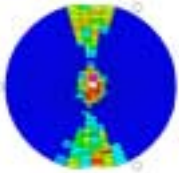	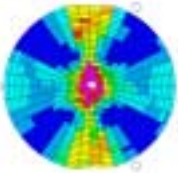	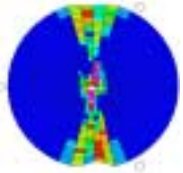	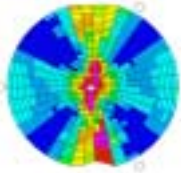

Highlighted regions indicate the average through-thickness damage state of fibre and matrix failure, respectively

Table 5. Contour plots of predicted fibre and matrix failure at the point of first structural failure for the composite discs using different punch diameters and composite lay-ups.

I. Appendix: Summary of Identified Material Parameters for Intra-laminar Ply Failure

	Notation	Symbol	Value
Elastic Properties	Fibre tension modulus	E_{11t}	*114 GPa*
	Fibre compression modulus	E_{11c}	*80 GPa*
	Matrix transverse modulus	E_{22}^{0}	*7.8 Gpa**
	Matrix shear modulus in 12-direction	G_{12}^{0}	*2.85 GPa*
	Matrix shear modulus in 23-direction	G_{23}^{0}	*2.50 Gpa**
	Poisson's ratio in 12-direction	υ_{12}^{0}	*0.32**
	Poisson's ratio in 21-direction	υ_{21}^{0}	*0.03**
	Fibre volume ratio	V_f	*0.48*
Plastic Properties	Matrix yield stress	R_0	*0.02 GPa*
	Matrix hardening coefficient	β	*0.67 GPa*
	Matrix hardening exponent	m	*0.52*
	Matrix anisotropy factor	a^2	*0.33*
Damage Properties	Initial shear damage threshold	$\overline{Y}_{12}^{0}$	*0.008 √GPa*
	Shear damage fitting parameter	$\overline{Y}_{12}^{fit}$	*0.035 √GPa*
	Damage state of saturation	d_{12}^{Sat}	*0.8*
	Initial transverse damage threshold	$\overline{Y}_{22}^{0}$	$\rightarrow\infty$
	Damage coupling factor	b	$\rightarrow 0$
Failure Properties	Maximum fibre tensile strain	$\varepsilon_{11,t}^{\max}$	*0.0155*
	Maximum fibre compression strain	$\varepsilon_{11,c}^{\max}$	*-0.01*
	Matrix transverse tensile strength	$R_{\perp}^{(+)}$	*0.050 GPa**
	Matrix transverse compression strength	$R_{\perp}^{(-)}$	*0.180 GPa**
	Matrix shear strength	$R_{\perp\parallel}$	*0.060 GPa*
	Failure envelope fitting parameter	$p_{\perp\parallel}^{(+)}$	*0.43*
	Failure envelope fitting parameter	$p_{\perp\parallel}^{(-)}$	*0.01*

*) Estimated values [15]

Table 6. Summary of identified material model parameters for biaxial carbon/epoxy NCF composite.

Paper: Composites Science and Technology

Modelling damage and failure in carbon/epoxy Non Crimp Fabric composites including effects of fabric pre-shear

L. Greve Volkswagen AG, Group Research, 38436 Wolfsburg, Germany

A. K. Pickett* School of Industrial and Manufacturing Science, Cranfield University, Bedford, MK43 0AL, United Kingdom

Abstract

A numerical material model for intra-laminar failure prediction of biaxial Non Crimp Fabric composites is presented. The model combines the elasto-plastic continuum damage constitutive model proposed by Ladevèze with the intra-laminar matrix failure model of Puck, and improves the shear damage representation using an exponential damage function. The work focuses on numerical model development for damage and failure prediction and validation for both unsheared and sheared fabric composites which will result from draping of the fabric preform over a double curved geometry in order to manufacture complex shaped parts. An extensive test program has been conducted using flat composite coupons with differing degrees of fabric pre-shear in order to establish a database of material stiffness, strength, and in-plane matrix shear damage evolution prior to failure. This database is used to identify parameters for the proposed 'Ladevèze-Puck' damage and failure model. Final validation has been made by implementing the model in an explicit Finite Element code and performing a series of experimental and simulation analyses on transversely loaded circular composite discs having differing degrees of fabric pre-shear. The model has been shown to successfully capture intra-ply failure modes in the principle fibre directions for tension and compression, intra-ply shear and also the interaction of these modes.

Keywords

A. Polymer-matrix composites (PMC's)
B. Strength
C. Computational modelling
D. Mechanical testing

* Author for correspondence: Email a.k.pickett@cranfield.ac.uk

E. Nomenclature

Symbol	Description
$\{\boldsymbol{\sigma}\}$	Stress vector in the material co-ordinate system.
$\{\boldsymbol{\varepsilon}^e\}$	Elastic strain vector
$[\mathbf{C}]$, C_{ij}	Stiffness matrix and component.
ε_{ij}^e, ε_{ij}^p, ε_{ij}^t	Elastic, plastic, and total strain vector component.
E_{ij}^0, G_{ij}^0, υ_{ij}^0	Initial elastic modulus, shear modulus, and Poisson's ratio.
d_{ij}	Damage function.
Y_{ij}	Damage conjugate quantities.
b	Damage coupling coefficient.
$\overline{Y}$	Damage governing equation.
$\overline{Y}_{ij}^k$	Fitting parameters for damage functions.
W_e^0, W_e^d	Initial and damaged internal energy.
$\langle x \rangle_+$	Operator returning expression x if x is positive and 0 otherwise.
$sup_{\tau \in t}(x)$	Supreme of x: Maximum of x within the time frame $0 \le \tau \le t$.
G_{iC}	Critical strain energy release rate.

Symbol	Description
f	Yield function.
$\{\tilde{\sigma}\}$, $\tilde{\sigma}_{ij}$	Effective stress vector and component.
a	Anisotropy coefficient for yield function.
R_0, β, m	Yield stress, and hardening curve parameters (Ladevèze model).
$\varepsilon_{11,t}^{\max}$, $\varepsilon_{11,c}^{\max}$	Maximum fibre strain in tension and compression.
$\{\boldsymbol{\sigma}^{fail}\}$, σ_{ij}^{fail}	Matrix failure stress vector and component.
$\lambda_{Mode\ i}$	Mode dependent scaling distance to matrix failure envelope.
$R_{\perp}^{(+)}$, $R_{\perp}^{(-)}$, $R_{\perp\parallel}$	Basic strength in matrix transverse tension, transverse compression, and matrix shear direction.
$p_{\perp\parallel}^{(+)}$, $p_{\perp\parallel}^{(-)}$	Slope parameter of Puck fracture curve in transverse tension and transverse compression direction.
φ	Fibre orientation angle.
V_f	Fibre volume fraction.

1. Introduction

Advanced composites using Non Crimp Fabrics (NCF) and Liquid Composite Moulding (LCM) technologies are becoming increasingly attractive to the automotive (and other) industries for the economical manufacture of high performance parts in small series production runs. The absence of crimp gives high specific stiffness and strength, and biaxial NCF textile forms offer excellent drapeability for the manufacture of complex shapes. However, predictive failure models for these composites, suitable for impact and crash analysis, which can also account for fabric preshear, is required.

The potential intra-laminar failure modes of biaxial NCF are failure in one of the two fibre directions; either in tension or compression, and intra-laminar shear failure leading to fibre-matrix debonding. Lamina transverse matrix failure might also be observed; however, this mode will not initiate catastrophic ply failure since loading will be effectively transferred by the orthogonal tows of the adjacent plies. This is an observation recognised by Hart-Smith [1] in failure criteria he developed for

Unidirectional (UD) cross plies composites. A further possible composite failure mode is ply delamination; which has been investigated in a previous publication by the authors []. This failure mode is not considered here.

The excellent drapeability of NCF's allows both single and complex double curvature shapes to be formed, Figure 1. The shaping operation may cause extensive fabric shearing which will significantly modify local composite stiffness and strength properties. In excessively sheared areas fibre alignment will enhance strength in the fibre directions and render the composite vulnerable to failure under combined tension-shear loading in the transverse direction, Figure 1. For the work presented here a ±45° biaxial NCF having the specifications shown in Table 1 is used.

During the past three decades many composites failure models have been proposed and several have found their way into commercial Finite Element (FE) codes for prediction of ply failure. A recent comprehensive study to evaluate the most promising of these has been presented [2] Greve L, Pickett AK, "Delamination testing and modelling for composite crash simulation", Composites Science and Technology, in press, 2005.
[]. From this study the 'Puck' model [] was highly rated and has been considered "*to be the best at capturing the qualitative characteristics of lamina and laminate behaviour*" []. However, it was noted that this theory neglected inelastic material deformations which led to significant underestimation of strains for matrix dominated load cases. A further noteworthy contribution to this study was by Cuntze [] who, in many respects used a similar model to 'Puck' [], but also accounted for matrix plasticity.

The constitutive model proposed by Ladevèze and Le Dantec [] allows representation of matrix plasticity, combined with matrix damage; thus providing an improved basis for prediction of the stress-strain relation of the material. This paper presents a combination of the 'Ladevèze' model and the 'Puck' failure criteria to treat in-plane failure of carbon NCF reinforced composites under combined loading conditions; further improvements for representation of matrix shear damage development in NCF composites have also been necessary. The next section introduces the failure models, followed by sections on parameter identification and validation. Both unsheared and pre-sheared fabric composites have been considered in the experimental and numerical work. It is believed that the techniques presented are, in principle, also applicable to other biaxial textile reinforced composites such as conventional woven fabrics.

2. Material Modelling

2.1. The damage constitutive model

The classical continuum damage mechanics model proposed by Ladevèze and Le Dantec has been implemented in a multi-layered thin shell element in the explicit Finite Element code PAM-CRASH™ []. This allows each ply in the laminate to be represented using an orthotropic elasto-plastic, with damage, stress-strain relationship given by,

$$\{\boldsymbol{\sigma}\} = [\mathbf{C}]\{\boldsymbol{\varepsilon}^e\}. \tag{2-1}$$

The stress and strain vectors are,

$$\{\sigma\}^T = \{\sigma_{11} \quad \sigma_{22} \quad \sigma_{12} \quad \sigma_{23} \quad \sigma_{31}\}^T,$$

and

$$\{\boldsymbol{\varepsilon}^e\}^T = \{\varepsilon^e_{11} \quad \varepsilon^e_{22} \quad \varepsilon^e_{21} \quad \varepsilon^e_{23} \quad \varepsilon^e_{31}\}^T,$$

and the stiffness matrix [**C**] has the following form and coefficients,

$$[\mathbf{C}] = \begin{bmatrix} C^0_{11} & \upsilon^0_{21}C^0_{11} & 0 & 0 & 0 \\ \upsilon^0_{21}C^0_{11} & C^0_{22}(1-d_{22}) & 0 & 0 & 0 \\ 0 & 0 & G^0_{12}(1-d_{12}) & 0 & 0 \\ 0 & 0 & 0 & G^0_{23}(1-d_{12}) & 0 \\ 0 & 0 & 0 & 0 & G^0_{12}(1-d_{12}) \end{bmatrix}, \tag{2-2}$$

with

$$C^0_{11} = \frac{E^0_{11}}{1-\upsilon^0_{12}\upsilon^0_{21}} \quad ; \; C^0_{22} = \frac{E^0_{22}}{1-\upsilon^0_{12}\upsilon^0_{21}}.$$

In the above equations the material constants E^0_{11} and E^0_{22} are elastic modulii in the fibre and transverse directions, G^0_{ij} is shear modulus, and υ^0_{ij} is Poisson's ratio. The matrix dominated elastic modulii, $E_{22}{}^0$, $G_{12}{}^0$, and $G_{23}{}^0$, are modified by the damage functions ($1\text{-}d_{ij}$) during loading to failure. Two scalar damage functions d_{22} and d_{12} are introduced, having the range 0 (no damage) to 1.0 (fully damaged) to describe matrix damage development in the ply transverse and shear directions, respectively. Some simplifications for numerical implementation are made for out-of plane shear modulii. Based on the assumption of transverse isotropy, the shear modulus in the 1-2 and 1-3 directions are considered equal, $G_{13}{}^0 = G_{12}{}^0$. Consequently, equal damage development in both directions is assumed, $d_{13} = d_{12}$. For the sake of simplicity shear damage in the 2-3 direction is related to in-plane shear damage development, $d_{23} = d_{12}$. The theory assumes constant Poisson's ratio coefficients.

The damage functions (d_{22} and d_{12}) are associated with conjugate quantities Y_{22} and Y_{12}, which govern damage development. These quantities are partial derivatives of damaged elastic work with respect to

the damage state and are analogous to the strain energy release rate G_{ic} used in classical Fracture Mechanics to describe strain energy released during crack growth []. The expressions for Y_{12} and Y_{22} are,

$$Y_{12} = \frac{\partial W_e^d}{\partial d_{12}} = \frac{\partial}{\partial d_{12}} \frac{1}{2} \{\boldsymbol{\varepsilon}^e\}^T [\mathbf{C}] \{\boldsymbol{\varepsilon}^e\} = \frac{1}{2} \left\{ G_{12}^0 \left[\left(\gamma_{12}^e\right)^2 + \left(\gamma_{13}^e\right)^2 \right] + G_{23}^0 \left(\gamma_{13}^e\right)^2 \right\}, \tag{2-3}$$

$$Y_{22} = \frac{\partial W_e^d}{\partial d_{22}} = \frac{\partial}{\partial d_{22}} \frac{1}{2} \{\boldsymbol{\varepsilon}^e\}^T [\mathbf{C}] \{\boldsymbol{\varepsilon}^e\} = \frac{1}{2} C_{22}^0 \left(\left\langle \upsilon_{12}^0 \varepsilon_{11}^e + \varepsilon_{22}^e \right\rangle_+ \right)^2, \tag{2-4}$$

where the operator $<...>_+$ distinguishes transverse tension and compression as follows,

$$\left\langle x \right\rangle_+ = \begin{cases} x & if\,(x > 0) \\ 0 & otherwise \end{cases}. \tag{2-5}$$

Damage development under matrix transverse compression loading is prohibited, equation (2-4), due to the assumption that existing matrix micro-cracks will close under compression loading, in which case the initial transverse elastic modulus is recovered. Damage interaction is introduced by the parameter b, leading to the final governing equation for coupled transverse-shear damage,

$$\overline{Y}(t) = \sup_{\tau \le t} \left(\sqrt{Y_{12}(\tau) + b Y_{22}(\tau)} \right). \tag{2-6}$$

Generally the coupling factor b is determined from experiments.

Enhancements to shear damage representation for NCF

A lamina under pure in-plane intra-laminar shear loading will exhibit matrix micro-cracks after a certain threshold stress is exceeded Figure 2a. These cracks will be normal to the direction of first principal stress and will extend until stopped by fibres crossing the crack paths. Continued loading will generate new parallel cracks, Figure 2b, until a saturated level of matrix micro-cracks is reached, Figure 2c. Further loading will cause micro-cracks to coalescence and form a macro-crack leading to material fracture Figure 2d. Based on these micro-mechanical considerations a corresponding macro-mechanical shear damaging law is proposed to approximate the real physical behaviour of the investigated NCF composite. An exponential shear damage function is used, in which the damage state asymptotically approaches the level of saturated damage, Figure 2e. Similar nonlinear shear damage development has also been observed and used for woven fabric pre-preg composites [] and biaxial braid composites [2]. In the nonlinear shear damage function, Figure 2, $\overline{Y}_{12}^0$ represents the initiation of shear damage, $\overline{Y}_{12}^{fit}$ is a fitting parameter for the shape of the shear damage evolution curve, and d_{Sat} represents the saturation damage level.

Matrix plasticity

A cyclic tensile coupon test of a $[\pm 45]_{2s}$ laminate is used to characterise evolution of matrix shear damage and plasticity. The global laminate stresses and strains are transformed to assess the local ply

shear stress-strain curve, Figure 3. The degradation of the ply shear modulus $G_{12,i}$ and the generation of inelastic ply deformation $\gamma_{12,i}^{p}$ can be clearly observed.

For NCF the plasticity model proposed by Ladevèze and Le Dantec for UD composites [] has been found appropriate and is used here. Briefly, this is simple Von Mises yield criteria using an associated flow rule to monitor the evolution of permanent plastic strains in the matrix caused by the transverse and shear strain components,

$$f = \sqrt{\tilde{\sigma}_{12}{}^{2} + a^{2}\tilde{\sigma}_{22}} - R(p) = 0\,, \tag{2-7}$$

with the effective stresses,

$$\tilde{\sigma}_{ij} = \frac{\sigma_{ij}}{1-d_{ij}}\,. \tag{2-8}$$

Factor a^2 can account for material anisotropy. Assuming an isotropic matrix material it can be shown from the 'Von Mises' yield condition that $a^2 = 1/3$.

A power law is assumed for plastic strain hardening,

$$R(p) = R_o + \beta p^m, \tag{2-9}$$

where R_0 is the shear yield stress, β and m are curve fitting parameters. The equivalent plastic strain p is given by,

$$p = \int (1-d_{12})\, d\gamma_{12}^{p}\,, \tag{2-10}$$

where the plastic shear strain increment $d\gamma_{12}^{p}$ is the difference between the total and elastic shear strain increments,

$$d\gamma_{12}^{p} = d\gamma_{12}^{t} - d\gamma_{12}^{e}\,. \tag{2-11}$$

Material parameter identification

The shear damage development and plastic hardening curve are determined by quasi-static cyclic tensile testing of $[\pm 45]_{2s}$ NCF composite coupons to failure, Figure 4. A rate of loading of 0.5 mm/min in an Instron 5500R-6025 testing machine has been used. The parameter identification for shear follows the procedures outlined in [] with the new exponential shear damage function. Figure 5a,b shows the good fit of damage and hardening functions to experimental data points. For this work the exponential shear damage function has been implemented and used in a research version of the FE code PAMCRASH™.

The calibrated model parameters are summarised in Appendix I. Simulation of the cyclic tensile test using the new exponential damage function yields very good agreement with the experimental results, as shown by comparison of the longitudinal stress-strain curves in Figure 5c. Another simulation

curve, computed using the original linear damaging function, is included for comparison. The linear damage approach leads to higher stresses at the beginning due to the underestimation of the damage state, Figure 5a. Furthermore, premature specimen failure is observed in this simulation once damaging localises and approaches the limiting value 1.0.

The original 'Ladevèze' model allows coupling of transverse tension damage and shear damage; $b \neq 0$ in equation (2-6). However, since carbon/epoxy biaxial NCF composites exhibit brittle elastic transverse tensile failure without significant damaging it is assumed that transverse deformation does not contribute to shear damage development; thus shear damage development is solely governed by shear deformation; $b \to 0$.

2.2. The Intra-laminar failure model

Fibre dominated failure: The elastic lamina modulii in the fibre direction ($E_{11t,c}$) and the corresponding maximum elastic strains ($\varepsilon_{11t,c}^{\max}$) have been obtained using standard tension and compression tests of $[0/90]_{2s}$ NCF coupons according to ASTM standards [3] and [4], Figure 6. The material model parameters obtained from these tests are summarised in Appendix I.

Matrix dominated failure: The in-plane intra-laminar matrix failure envelope proposed by Puck for a unidirectional lamina is represented by three different inter-connected curve functions, each representing a distinct failure mode A, B, and C, as shown in Figure 7.

The original 'Ladevèze' model contains a failure criterion for matrix failure which is directly related the to damage development []. As previously mentioned, only shear damage is assumed to be active occur under transverse compression loading, giving an open matrix failure envelope in the transverse compression direction, Figure 8. This is felt to be inappropriate for the NCF composite investigated here; although it is noted that recent work by Ladevèze et al. [5], has enhanced this failure mode to include transverse compression. In this work, however, the established 'Puck' failure criterion is preferred, so that matrix damage development and the matrix failure criterion are completely uncoupled.

For numerical integration of the Puck matrix failure criterion into an FE code it is convenient to use a scaling distance λ, defined as the ratio of the current stress vector $\{\boldsymbol{\sigma}\}$ to the extrapolated vector at the failure envelope $\{\boldsymbol{\sigma}^{\text{fail}}\}$, Figure 8, such that,

$$\{\boldsymbol{\sigma}\} = \lambda\{\boldsymbol{\sigma}^{fail}\}, \tag{2-12}$$

with

$$\lambda = \begin{cases} <1 & no\ failure \\ 1 & failure \\ >1 & post-failure \end{cases}. \tag{2-13}$$

Based on the equations for matrix failure [6] the maximum λ for the different failure modes follows as,

$$\lambda = \begin{cases} \lambda_{ModeA} & if\left(\sigma_{22} \geq 0\right) \\ \lambda_{ModeB} & if\left(\sigma_{22} < 0 \quad and \quad 0 \leq \left|\frac{\sigma_{22}}{\sigma_{12}}\right| \leq \left|\frac{R^{A}_{\perp\perp}}{\sigma_{12c}}\right|\right) \\ \lambda_{ModeC} & if\left(\sigma_{22} < 0 \quad and \quad 0 \leq \left|\frac{\sigma_{12}}{\sigma_{22}}\right| \leq \left|\frac{R^{A}_{\perp\perp}}{\sigma_{12c}}\right|\right) \end{cases}. \tag{2-14}$$

With,

$$\begin{aligned} \lambda_{ModeA}(t) &= \sup_{\tau \leq t}\left[\frac{p^{(+)}_{\perp\|}R^{(+)}_{\perp}\sigma_{22}(\tau)+\sqrt{\left(R^{(+)}_{\perp}\right)^2(\sigma_{12}(\tau))^2+(\sigma_{22}(\tau))^2\left(R_{\perp\|}-p^{(+)}_{\perp\|}R^{(+)}_{\perp}\right)^2}}{R_{\perp\|}R^{(+)}_{\perp}}\right], \\ \lambda_{ModeB}(t) &= \sup_{\tau \leq t}\left[\frac{p^{(-)}_{\perp\|}\sigma_{22}(\tau)+\sqrt{(\sigma_{12}(\tau))^2+\left(\sigma_{22}(\tau)p^{(-)}_{\perp\|}\right)^2}}{R_{\perp\|}}\right], \\ \lambda_{ModeC}(t) &= \sup_{\tau \leq t}\left[\frac{-R^{(-)}_{\perp}(\sigma_{12}(\tau))^2}{4\left(1+p^{(-)}_{\perp}\right)^2\left(R_{\perp\|}\right)^2\sigma_{22}(\tau)}-\frac{\sigma_{22}(\tau)}{R^{(-)}_{\perp}}\right], \end{aligned} \tag{2-15}$$

and,

$$\begin{aligned} R^{A}_{\perp\perp} &= \frac{R_{\perp\|}}{2p^{(-)}_{\perp\|}}\left(\sqrt{1+2p^{(-)}_{\perp\|}\frac{R^{(-)}_{\perp}}{R_{\perp\|}}}-1\right), \\ \sigma_{12c} &= R_{\perp\|}\sqrt{1+2p^{(-)}_{\perp\perp}}, \\ p^{(-)}_{\perp\perp} &= p^{(-)}_{\perp\|}\frac{R^{A}_{\perp\perp}}{R_{\perp\|}}. \end{aligned} \tag{2-16}$$

The material model parameters used in these formulae represent the material strength in pure loading directions, $R^{(-)}_{\perp}$, $R^{(+)}_{\perp}$, and $R_{\perp\|}$, and several curve fitting parameters, $p^{(+)}_{\perp\|}$, and $p^{(-)}_{\perp\|}$, representing the slopes of the fracture curve at $\sigma_{22} = 0$ in positive and negative transverse direction, respectively [6].

Calibration of the failure envelope for pre-sheared NCF

An investigation to assess failure of pre-sheared NCF composites under combined loading is undertaken. Testing coupons were manufactured from dry orthotropic biaxial NCF which were manually pre-sheared from ±45° to ±φ° and stacked in a sequence of $[\pm\varphi]_{2s}$ prior to Vacuum Assisted Resin Infusion (VARI). The coupons were then cut from the manufactured panels, providing different

lay-up's ($[\pm\varphi]_{2s}$, $[\pm(90\text{-}\varphi)]_{2s}$, and $[0/2\varphi]_{2s}$) as indicated in Figure 9a. Two different pre-sheared composites were investigated; the first representing moderate fabric pre-shear ($\varphi = 35°$) and the second representing greater pre-shear ($\varphi = 28°$). The laminate thickness has been increased according to the amount of pre-shear in order to keep the fibre volume ratio approximately constant at $V_f = 0.48$ throughout the test programme.

Flat coupons were used for tension and compression testing using the procedures in [3] and [4] respectively, Figure 9b,c. All specimens were tested quasi-statically at 0.5 mm/min to failure in an Instron 5500R-6025 testing machine. The full testing programme undertaken is summarised in Figure 9d. Specimens tested in the fibre directions used monotonic loading to failure in tension and compression. The remaining specimens, $[\pm\varphi]_{2s}$ and $[\pm(90\text{-}\varphi)]_{2s}$, were tested using cyclic tension loading to failure in order to determine damage evolution and plasticity prior to failure. Table 1 summarises all results for fibre (tension and compression), and the cyclic shear failure cases.

Test results show an extensive nonlinear inelastic response for the $[\pm28]_{2s}$ and $[\pm35]_{2s}$ symmetric cyclic tension test coupons. Tension testing of the $[\pm55]_{2s}$ and $[\pm62]_{2s}$ coupons leads to a more linear elastic longitudinal stress-strain relation due to the increased contribution of elastic transverse loading. Specimens loaded in the fibre direction, $[0/2\varphi]_{2s}$, generally exhibit brittle elastic failure under both tension and compression loading. For all these tensile tests it is noted that only minor experimental scatter is observed.

An inverse approach is used for the calibration of the matrix failure envelope. The procedure is visualised in Figure 10, and explained below.

The $[\pm\varphi]_{2s}$ and $[\pm(90\text{-}\varphi)]_{2s}$ tension tests are modelled using multi-layered shell Finite Elements in PAM-CRASH^{TM}, and simulated in order to determine the material model parameters for the matrix failure envelope. The simulations are stopped at the point of failure according to the maximum observed experimental longitudinal strain and stress traces (σ_{12} *versus*) of a ply element within the failure zone of each simulated test case are collected on to one chart, Figure 11. Within some simulations structural failure is initiated by fibre failure (denoted by square symbol in Figure 11). The remaining (circular) end points of the stress traces are used to 'fit' the 'Puck' failure envelope. Thus the puck failure envelope obtained is valid for all unsheared and pre-sheared NCF composites tested. The basic strength (σ_{22} for an individual ply) in transverse tension and compression direction cannot be determined from the biaxial NCF composite. Hence, these strengths have been estimated from tests on a unidirectional NCF having similar carbon/epoxy systems.

The material model parameters determined are summarised in Appendix I. For confirmation of this inverse material model parameter identification procedure, simulations of all test cases were repeated using the matrix failure model parameters identified. The computed stress-strain curves to failure are in good agreement with the experiments, Table 2.

3. Validation of Simulation Methodologies: Transversely Loaded Composite Discs

The previous section has outlined the test and material parameter identification procedures used to determine failure data for unsheared and pre-sheared NCF composites. This section describes a test that has been devised to validate the material models and material parameters.

The test involves circular composite discs of 120mm diameter which are simply supported on their perimeter and quasi-statically loaded transversely at their centre with a rigid hemispherical punch of 25mm or 50mm diameter. The discs rest on a slightly bevelled (15°) ring and are constrained by three concentric pins, Figure 12, to provide the simple support condition. The test setup was specially designed to realise rotational symmetry and minimise bearing effects on the boundary. The loading rate to failure was 0.5mm/min in an Instron 5500R-6025 testing machine. Different lay-ups, including unsheared and pre-sheared NCF, were used in this validation exercise.

Disc Manufacture and Testing: Flat panels of NCF composite were manufactured using the VARI process having lay-ups of $[0/90/\pm45]_s$, $[\pm45]_{2s}$, $[\pm38/\pm52]_s$, and $[\pm35]_{2s}$. The lay-up's $[\pm38/\pm52]_s$ and $[\pm35]_{2s}$ were generated by manually shearing ±45° biaxial fabrics. The circular discs were then cut from the finished panels and prepared for testing, Table 3. The punch force-displacement curves obtained from testing are summarised in Figure 13 and Figure 14.

All tests display a gradually increasing force until first structural failure. The 50mm diameter punch specimens tend to exhibit failure by a sudden crack developing between the punch and the outer rim of the disc, which leads to a rapid drop in force. The post failure force response displays significant residual strength after first structural failure since the large punch allows force redistribution away from the damage area beneath the punch. The smaller punch creates greater confined local damage as it penetrates the disc. Figure 15 shows typical final deformations of the composite discs after transverse loading by the large and the small punch. Only minor scatter is observed for tests using the larger punch, whereas more variation is found for the force-displacement curves of the smaller punch specimens. Most scatter is observed in the pre-sheared $[\pm38/\pm52]_s$ specimens.

Simulation of the Disc Tests: The composite discs have been modelled using an average element length beneath the punch of 4mm, Figure 16. The bevelled ring, including the pins and the punches, are all treated as rigid bodies. The punch is displacement driven in the transverse direction (normal to

the disc) and standard contact definitions are applied between the composite disc, the punch and the ring.

The proposed combined 'Ladevèze-Puck' material model is used to represent the composite discs. The shell element used is a multilayered element in which the fibre orientation for each ply is defined using material model parameters summarised in Appendix I. The experimental and predicted force-displacement curves are shown in Table 4, and computed contour plots of fibre and matrix damage are displayed in Table 5.

Discussion of Results: The simulation results of the discs can be divided into two principal structural failure types; namely, fibre dominated and matrix dominated failure. Fibre dominated structural failure is predicted for the $[0/90/\pm45]_s$, $[\pm45]_{2s}$ and, to a lesser extent, the $[\pm38/\pm52]_s$ discs; whereas matrix dominated failure is predicted for the $[\pm35]_{2s}$ discs. These predicted global failure modes are in good agreement with corresponding ultrasonic C-SCAN measurements of the tested discs, Figure 17.

Fibre dominated structural failure of $[0/90/\pm45]_s$, $[\pm45]_{2s}$ and $[\pm38/\pm52]_s$ discs: For the larger punch failure is indicated by sudden straight laminate cracks radiating between the disc centre and outer rim, whereas the smaller punch predicts localised disc penetration failure, Table 5. The predicted global failure patterns agree well with the experiments, previously shown in Figure 15. Furthermore, the predicted force-displacement curves for these tests are generally in good agreement with experimental results, Table 4.

Matrix dominated structural failure of $[\pm35]_{2s}$ discs: Matrix dominated structural failure is predicted for both punches, Table 5. In each case matrix damage originates beneath the punch and then gradually propagates toward the outer composite rim, structural failure occurs once the damage front approaches the bearing.

It is interesting to note that similar experimental force-displacement curves were obtained for both punch sizes for the $[\pm35]_{2s}$ discs. The predicted force-displacement curves for the $[\pm35]_{2s}$ discs exhibit earlier structural failure than the corresponding experiments. A likely reason is that mechanical failure data for intra-laminar matrix failure underestimates the true material strength. It has been observed experimentally that there is a size effect in that wider specimens provide greater strength and strain to failure. The cut face, especially for narrow coupons, provides a source of stress concentrations leading to premature failure; this condition is not representative of the semi-continuous material at the centre of the disc. Never-the-less, it is encouraging that this relatively simple and efficient Finite Element approach, using shell elements with average edge lengths suitable for large industrial FE analysis problems, can realistically predict failure for all the considered cases.

4. Conclusions

An experimental test programme using biaxial carbon/epoxy Non Crimp Fabric composites has been undertaken to establish a data set for matrix and fibre dominated damage and failure. Fabric pre-shear of biaxial NCF, potentially occurring during the preforming operation in complex shaped composite parts, has to be addressed in failure analysis since fibre re-orientation renders the composite vulnerable to catastrophic combined matrix transverse-shear failure. Hence, the experimental test series has included the investigation of both unsheared and presheared biaxial NCF having differing degrees of fabric pre-shear. From this data a new failure law has been proposed that combines the elasto-plastic damaging constitutive model of Ladevèze and Le Dantec with the intra-laminar matrix failure model by Puck. Based on physical considerations, an exponential shear damage function has been established, which allows an improved representation of the shear damage development in these materials. All simulation methodologies have been implemented and tested using a research version of the PAMCRASH^{TM} code.

The 'Puck' matrix failure envelope was successfully calibrated to account for failure of unsheared and pre-sheared biaxial NCF composites. The combined 'Ladevèze-Puck' model has been validated using unsheared and pre-sheared NCF composite discs subject to quasi-static transverse loading. These tests generated a variety of global failure mechanisms, which could be well predicted by numerical simulation. Furthermore, the overall agreement of experimental and predicted punch force-displacement curves has been encouraging. It is felt that the proposed test and simulation procedures would also be applicable to other biaxial fabric composites such as woven fabrics.

References

[1] Hart-Smith LJ, "Predictions of the original and truncated maximum-strain failure models for certain fibrous composite laminates", Composites Science and Technology, 1998, 58(7), pp. 1151-1178.

[2] Greve L, Pickett AK, "Delamination testing and modelling for composite crash simulation", Composites Science and Technology, in press, 2005.

[3] Harris B, Chou TW, Mai YW, Hinton MJ, Soden PD, Kaddour AS, "Failure criteria in fibre-reinforced polymer composites", Composites Science and Technology, Special Issue, Vol. 58, July 1998.

[4] Puck A, Schürmann H, "Failure analysis of FRP laminates by means of physically based phenomenological models", Composites Science and Technology, Volume 62, Issues 12-13, September-October 2002, pp. 1633-1662.

[5] Hinton MJ, Kaddour AS, Soden PD, ”A comparison of the predictive capabilities of current failure theories for composite laminates, judged against experimental evidence”, Composites Science and Technology, Vol. 62, Issues 12-13, September-October 2002, pp. 1725-1797.

[6] Cuntze RG, “The predictive capability of failure mode concept-based strength criteria for multi-directional laminates—part B”, Composites Science and Technology, Vol. 64, Issues 3-4, 2004, pp. 487–516.

[7] Hinton MJ, Kaddour AS, Soden PD, “Recommendations for designers and researchers resulting from the world-wide failure exercise”, Composites Science and Technology, Vol. 64, Issues 3-4, 2004, pp. 589–604.

[8] Ladevèze P, Le Dantec E, “Damage Modelling of the elementary ply for laminated composites”, Composites Science and Technology, Vol. 43, Issue 3, 1992, pp. 257-267.

[9] PAM-CRASH™ Users manuals, Engineering Systems International, 20 Rue Saarinen, Silic 270, 94578 Rungis-Cedex, France. www.esi-group.com

[10] Johnson AF, Pickett AK, Rozycki P, "Computational methods for predicting impact damage in composite structures", Composites Science and Technology, Vol. 61, Issue 15, 2001, pp. 2183-2192.

[2] Pickett AK, Fouinneteau MRC, “Material characterisation and calibration of a meso-mechanical damage model for braid reinforced composites”, Composites Science and Technology, In Press 2005.

[3] ASTM Standard (1995b), “Standard test method for tensile properties of polymer matrix composite materials”, D3039.

[4] ASTM Standard (1995a), “Standard test method for compressive properties of polymer matrix composite materials with unsupported gauge section by shear loading”, D3410/D3410M-94.

[5] Ladevèze P, Lubineau G, “On a damage meso-model for laminates: micro-mechanics basis and improvement”, Mechanics of Materials, 2002.

[6] Puck A, “Festigkeitsanalyse von Faser-Matrix-Laminaten : Modelle für die Praxis”, Hanser Verlag München Wien, 1996.

[7] Daniel IM, Ishai O, “Engineering mechanics of composite materials”, Oxford University Press, Inc., 1994, ISBN 0-19-507506-4.

Figures

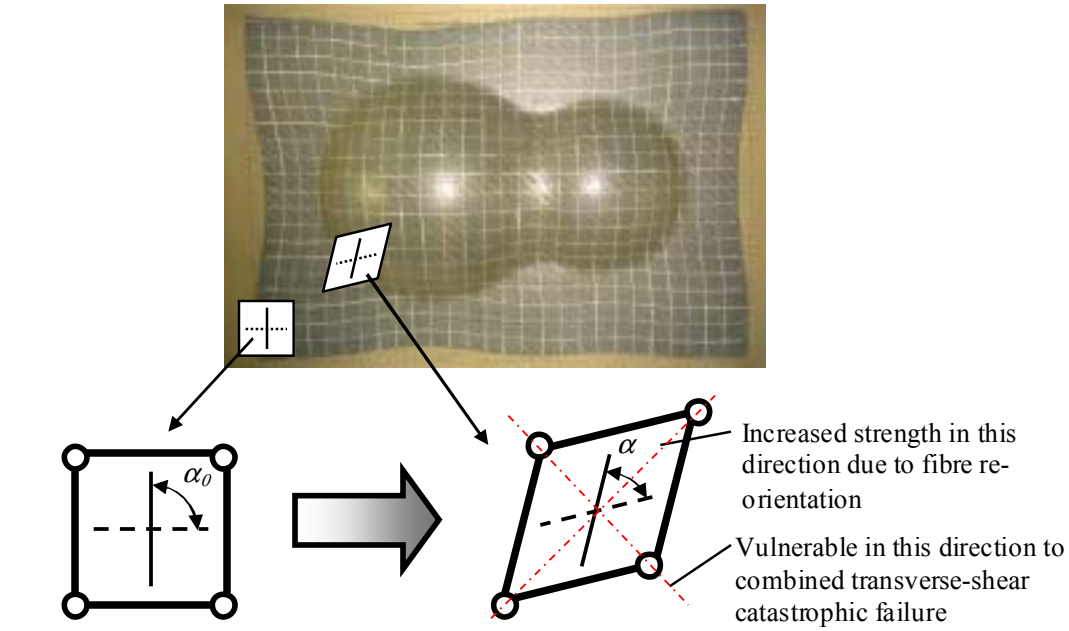

Figure 1. Fabric in-plane shear deformation of a biaxial (0/90) NCF due to draping over a double hemisphere surface.

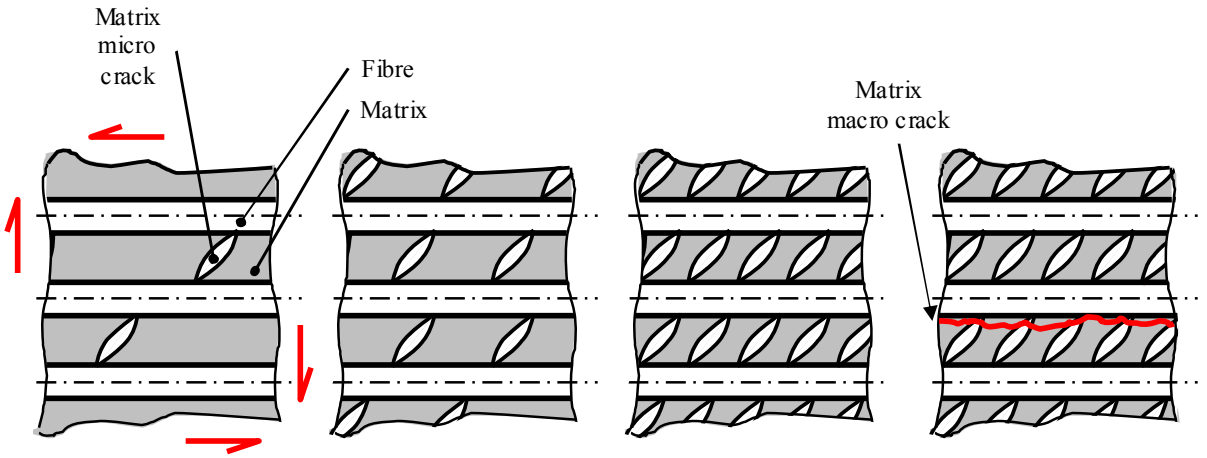

a) Initiation of matrix micro- shear cracking

b) Continuous matrix micro- shear cracking

c) Saturation of matrix micro-shear cracks

d) Formation of a macro- shear crack

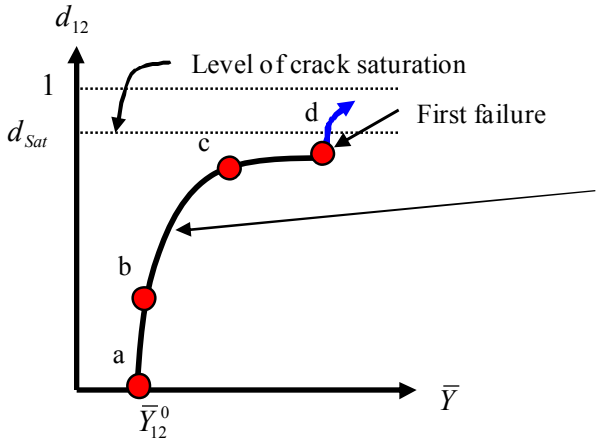

$$d_{12} = \begin{cases} d_{Sat}\left(1 - e^{\frac{\bar{Y}_{12}^{0} - \bar{Y}}{\bar{Y}_{12}^{fit}}}\right) & if\ \left(\bar{Y} > \bar{Y}_{12}^{0}\right) \\ 0 & otherwise \end{cases} \quad (4\text{-}1)$$

e) Macro-mechanical shear damage function for NCF representing the micro-mechanical failure phases (a-d)

Figure 2. Intra-laminar micro- and macro-crack formation under shear loading and corresponding shear damage function.

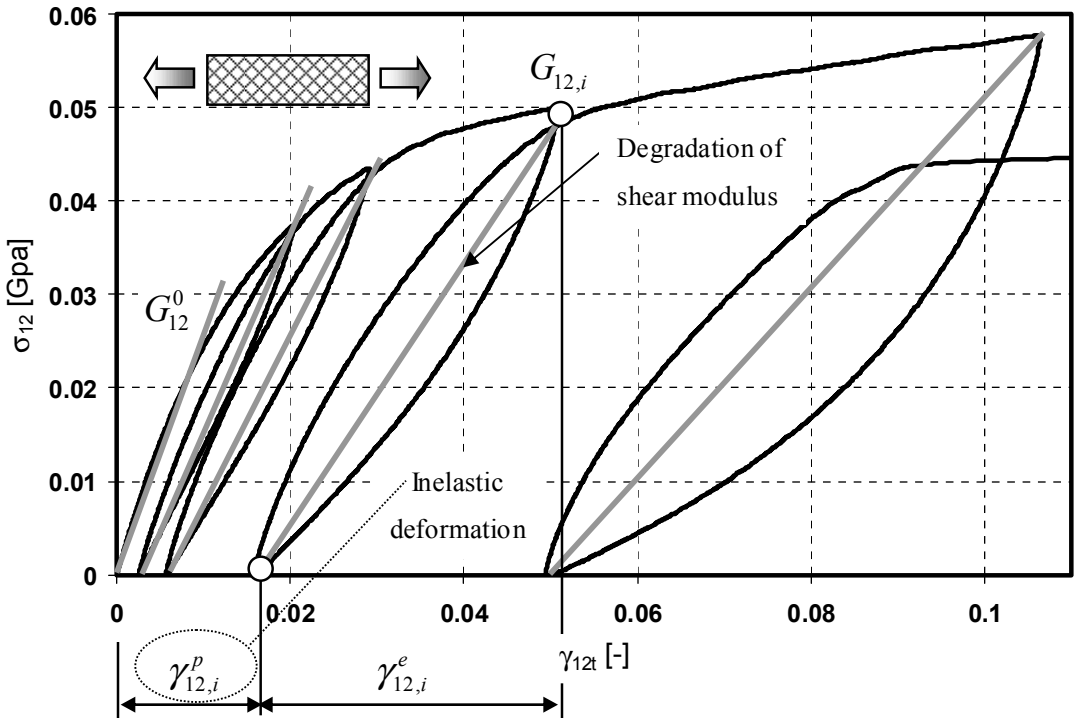

Figure 3. Lamina shear stress versus shear strain for a $[\pm 45]_{2s}$ cyclic tension coupon test.

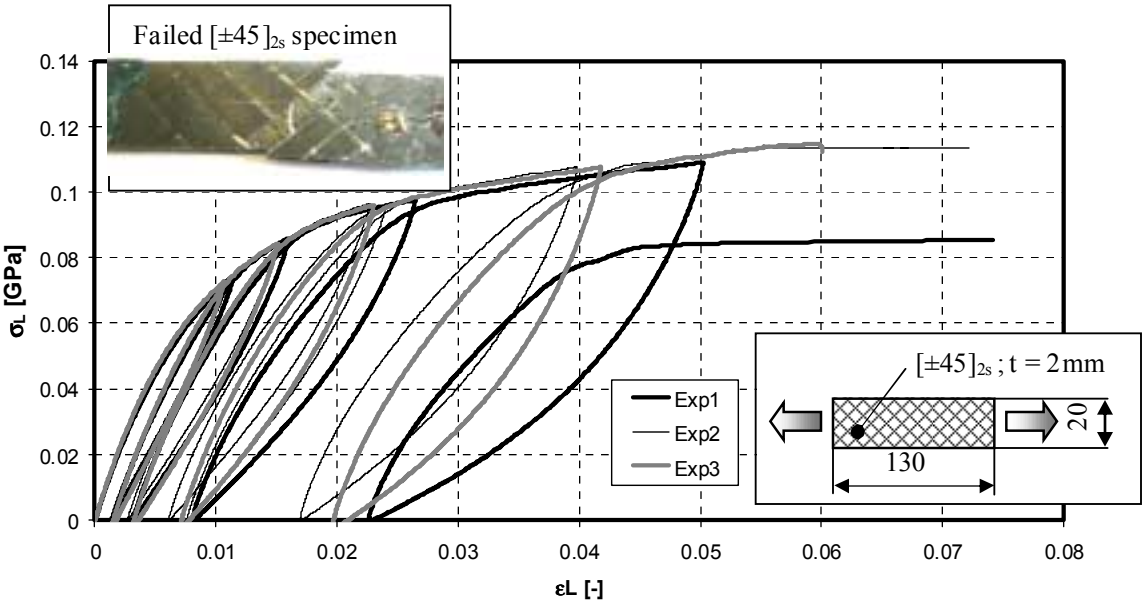

Figure 4. Longitudinal stress-strain curves for a cyclic tension $[\pm 45]_{2s}$ NCF coupon test.

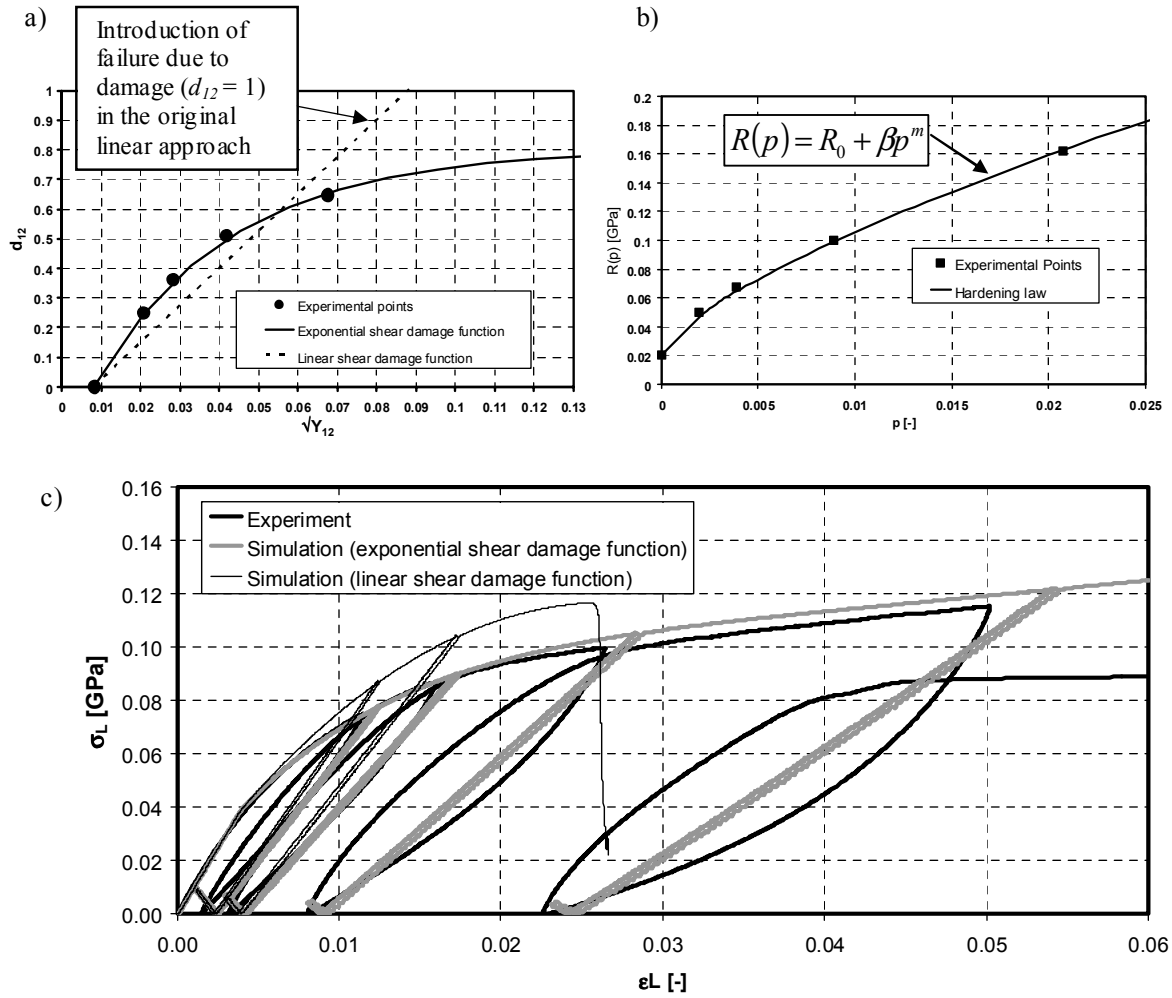

Figure 5. Calibration of the exponential shear damage function and plastic strain hardening curve:

a) Calibration of exponential and linear shear damage function

b) Calibration of plastic strain hardening function

c) Comparison of cyclic tension test and simulations using the original linear and new exponential damaging functions

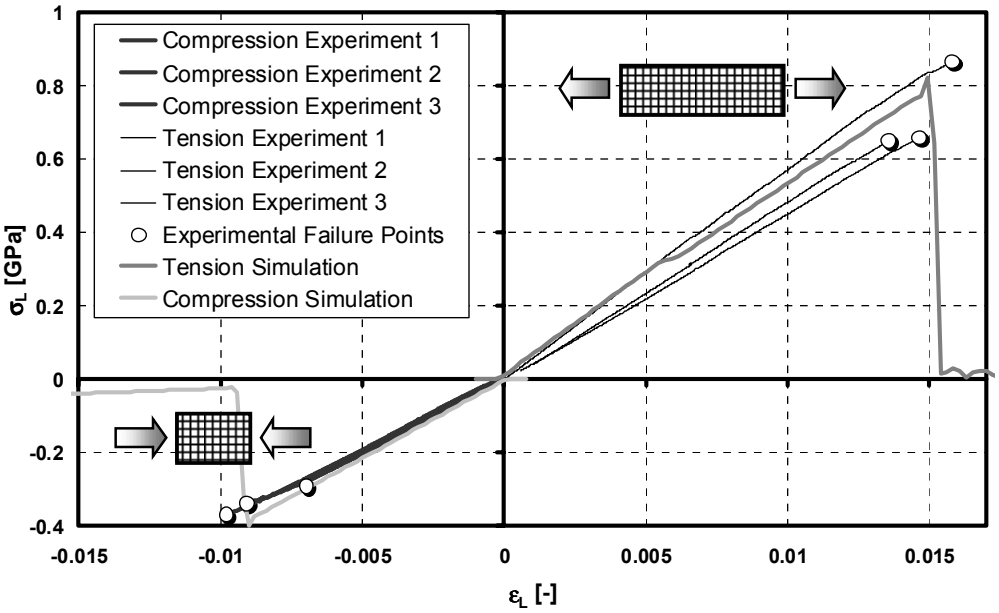

Figure 6. Tension and compression testing of $[0/90]_{2s}$ biaxial NCF coupons: Comparison of longitudinal stress-strain curves of experiments and simulations.

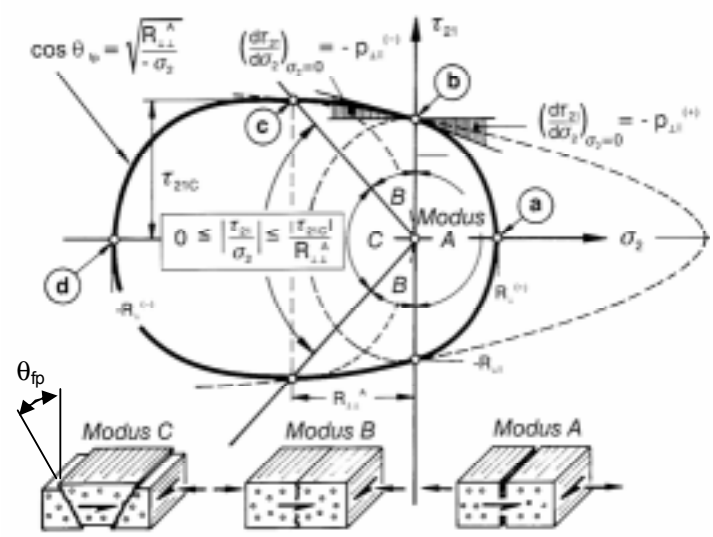

Figure 7. The 'Puck' matrix failure envelope in the in-plane matrix stress space [6].

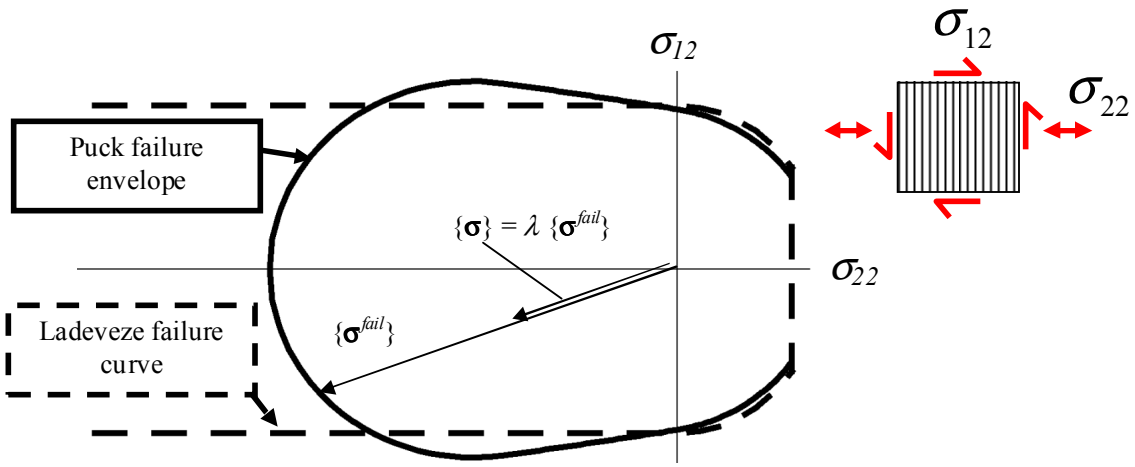

Figure 8. Principal comparison of the intra-laminar matrix failure curves proposed by Puck and Ladevèze.

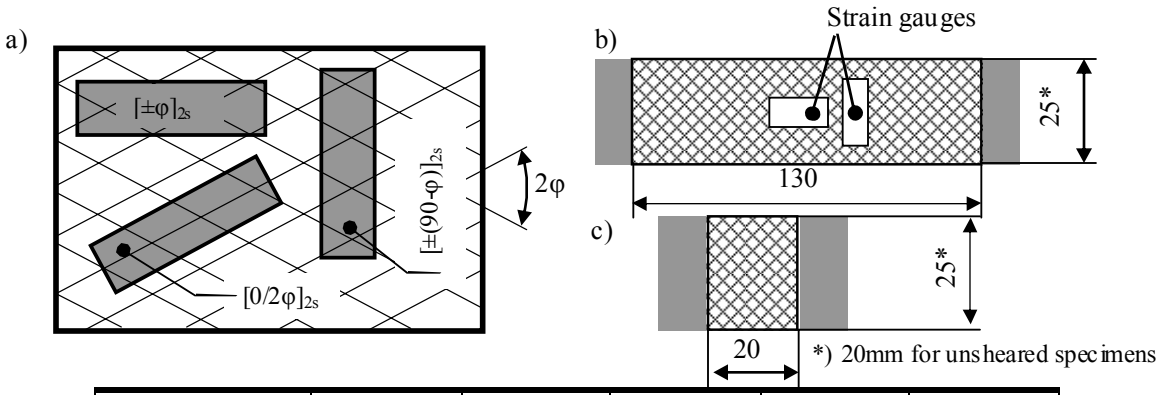

d)

Cyclic [±φ]2s tension	[±45]2s**	[±35]2s	[±28]2s	[±55]2s	[±62]2s
Sketch					
Thickness [mm]	2.0	2.1	2.6	2.1	2.6

**) Base fabric material (unsheared)

Simple [0/2φ]2s	[0/70]2s tension	[0/56]2s tension	[0/70]2s compr.	[0/56]2s compr.
Sketch				
Thickness [mm]	2.1	2.6	2.1	2.6

Figure 9. a) Specimen panels and cutting. b) Tension specimen dimensions. c) Compression specimen dimensions. d) Testing program of pre-sheared specimens.

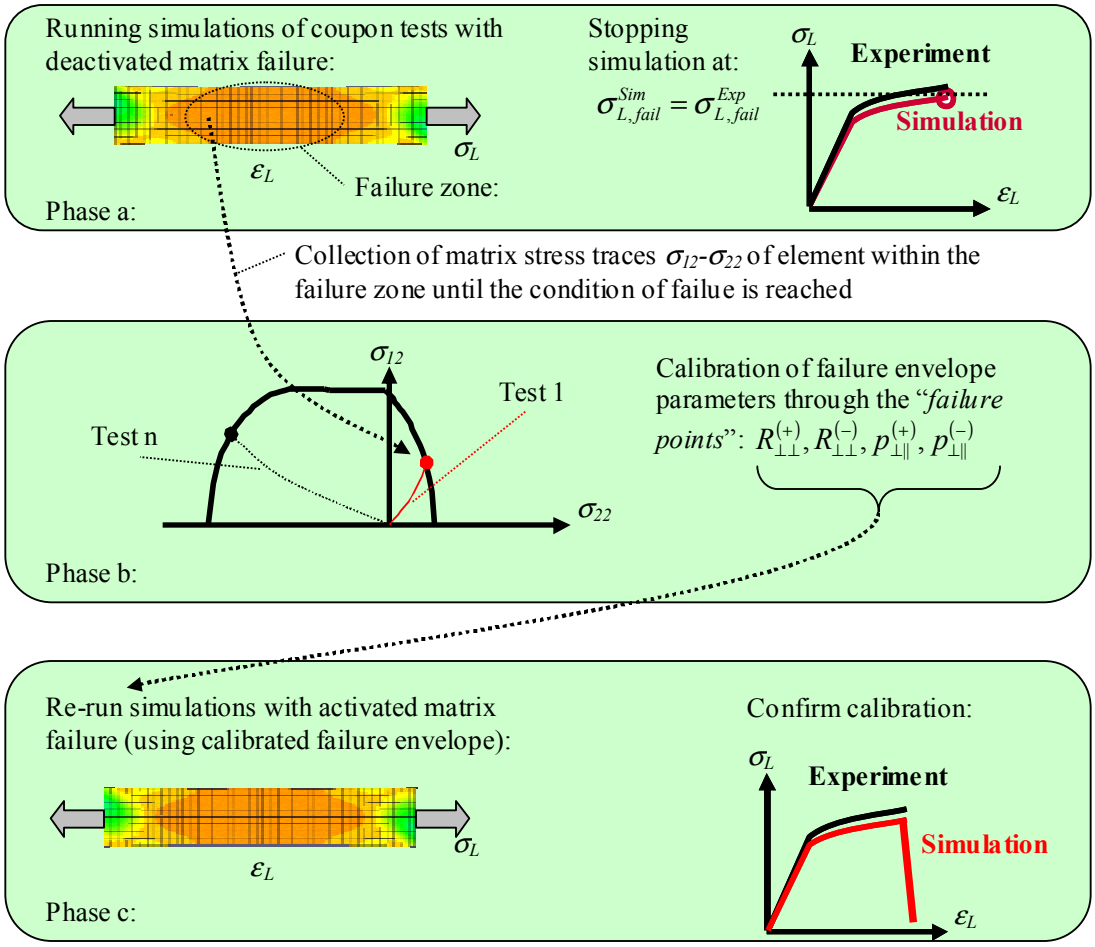

Figure 10. Procedure for the calibration of the matrix failure envelope using an inverse approach

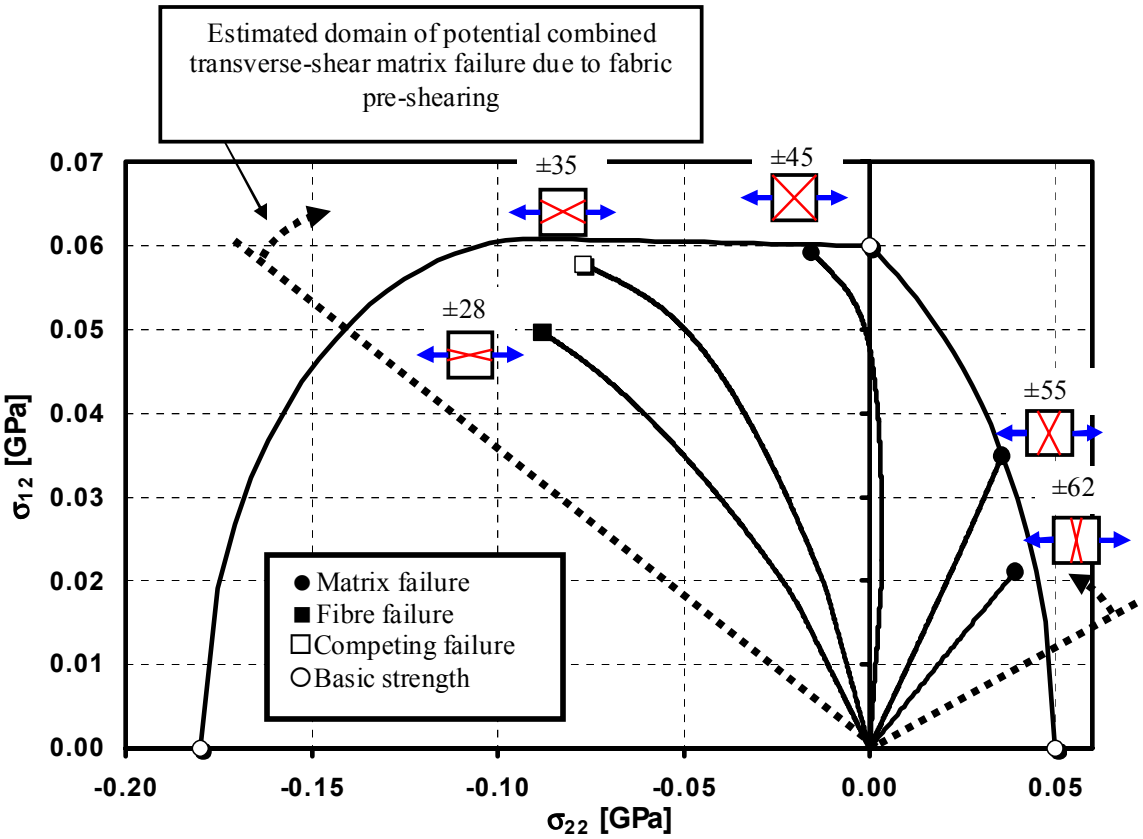

Figure 11. Stress traces of the $[\pm\varphi]_{2s}$ and $[\pm(90-\varphi)]_{2s}$ NCF coupons in the σ_{12}-σ_{22} space.

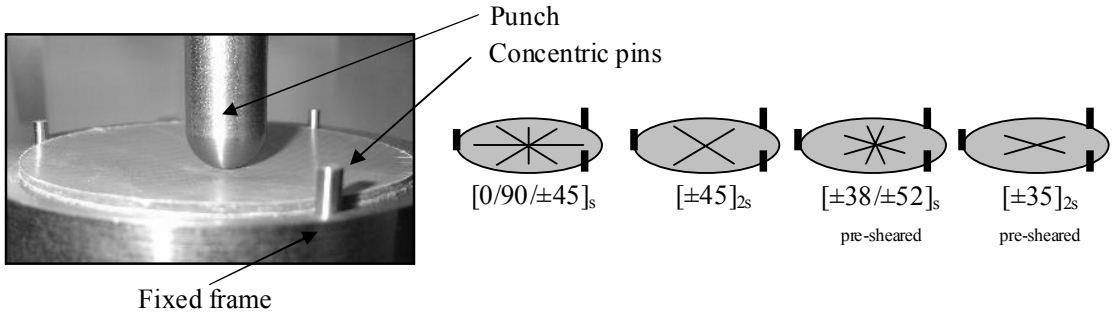

a) Test configuration and lay-ups

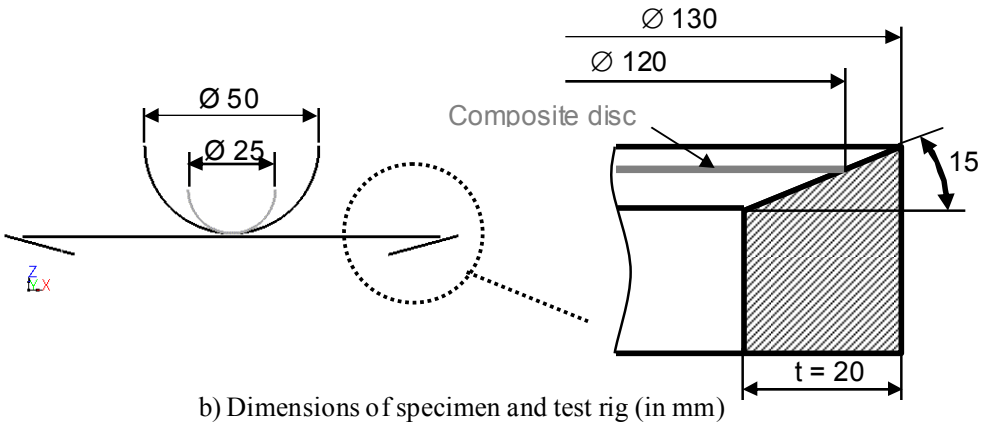

b) Dimensions of specimen and test rig (in mm)

Figure 12. Test configuration for the transversely loaded composite discs.

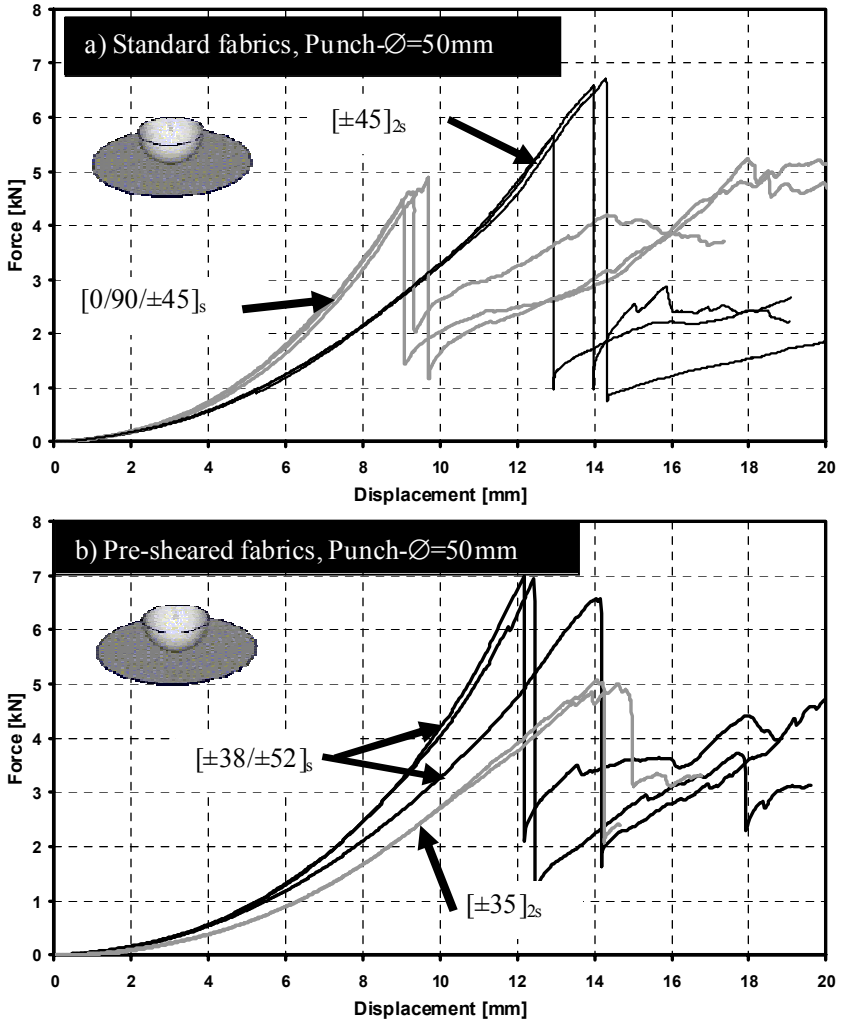

Figure 13. Experimental force-displacement curves for the composite discs subjected to quasi-static transverse loading to failure: Large punch (∅=50mm) results.

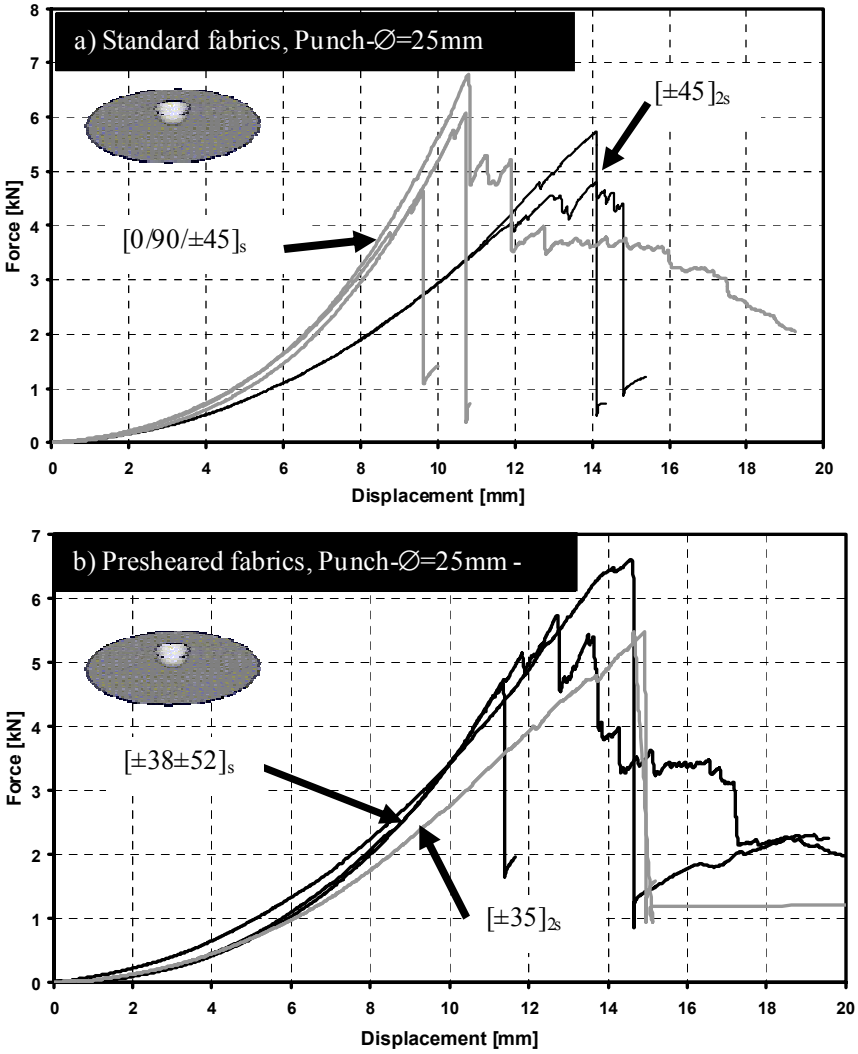

Figure 14. Experimental force-displacement curves for the composite discs subjected to quasi-static transverse loading to failure: Small punch (∅=25mm) results.

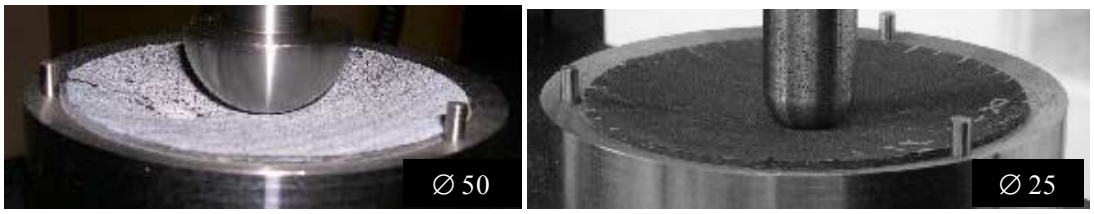

a) Failure deformations

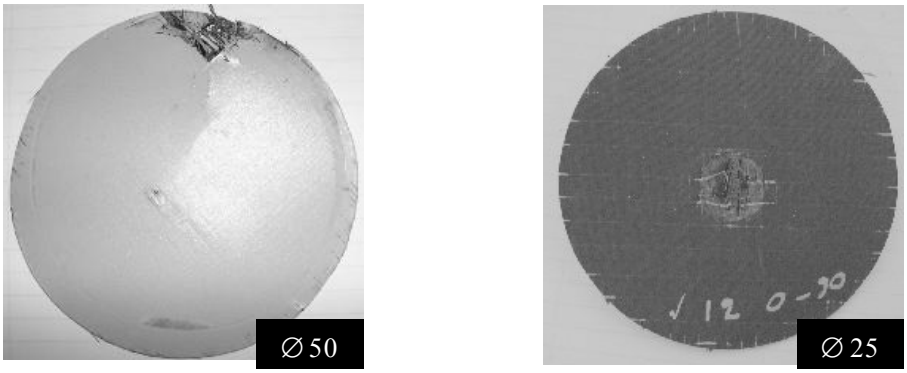

b) Final inelastic deformations (after spring-back)

Figure 15. Failure and final deformations of failed NCF composite disc specimens exemplarily shown for a $[0/90/\pm45]_s$ laminate.

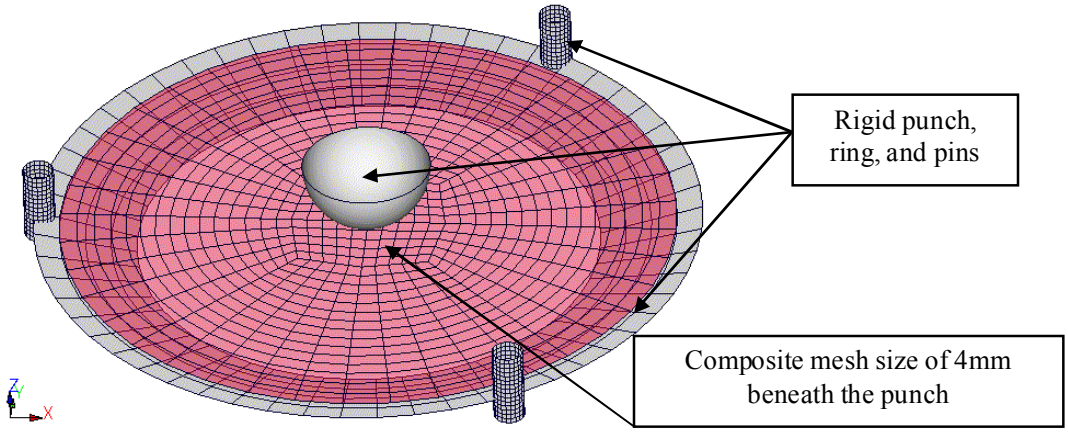

Figure 16. The setup and Finite Element model used for the transversely loaded NCF composite discs

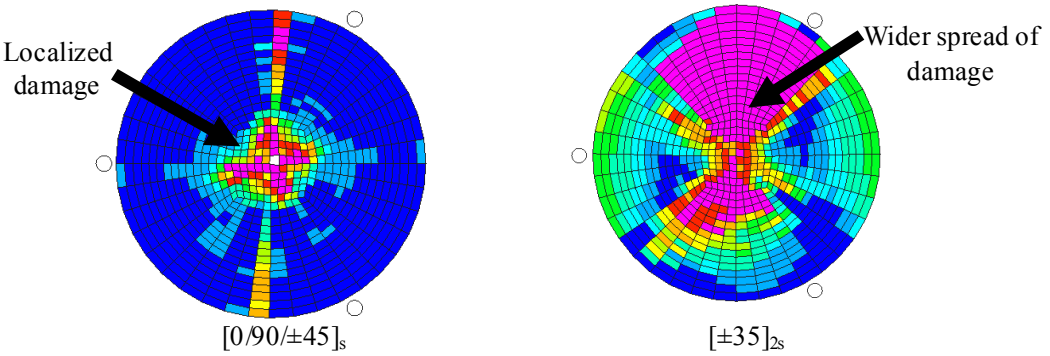

a) Qualitative comparison of computed average matrix damage development in a quasi-isotropic $[0/90/\pm45]_s$ NCF disc and a pre-sheared $[\pm35]_{2s}$ NCF disc transversely loaded using the large (∅50 mm) punch

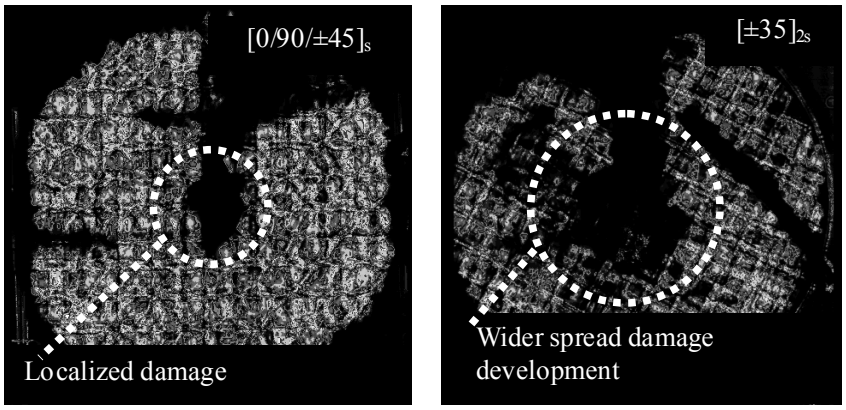

b) Ultrasonic C-Scans of the quasi-isotropic $[0/90/\pm45]_s$ NCF disc and the pre-sheared $[\pm35]_{2s}$ disc showing different degrees of internal damaging (dark regions) after transverse loading with the (∅=50 mm) punch

Figure 17. Comparison of computed matrix damage development and ultrasonic C-Scans for the NCF composite discs.

Tables

2-layer biaxial (±45) Non-Crimped Fabric	Specification
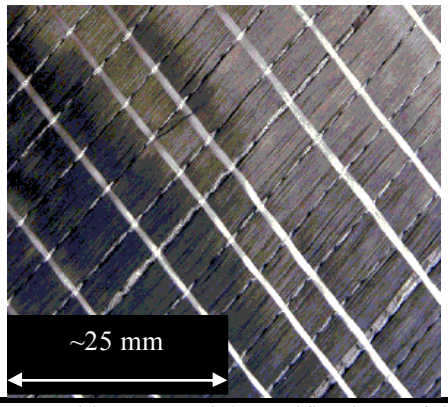	***Fabric Type:*** Biaxial 0/90 NCF fabric (m = 420 g/m²) 24k TORAY T600, carbon fibre Manufacturer: Saertex ***Epoxy System:*** LY 564 / HY2962 Fibre volume fraction: approx. 48 Vol.%

Table 4. Material specifications of the biaxial NCF carbon/epoxy composite material

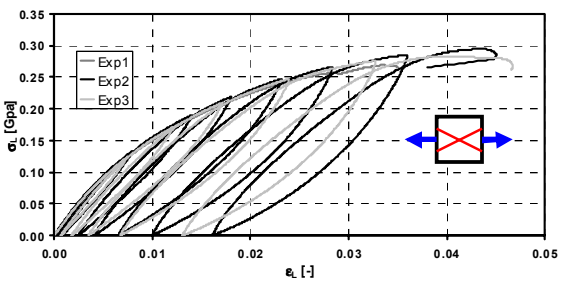

$[\pm 35]_{2s}$ cyclic tension

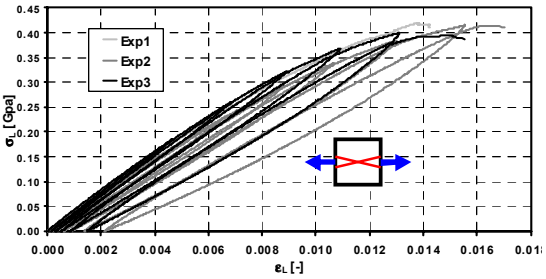

$[\pm 28]_{2s}$ cyclic tension

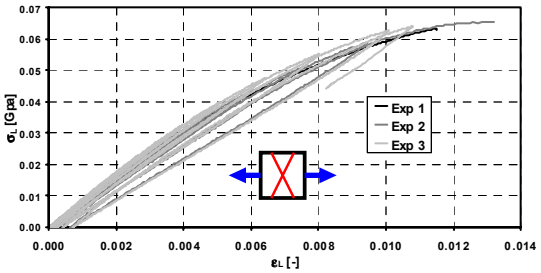

$[\pm 55]_{2s}$ cyclic tension

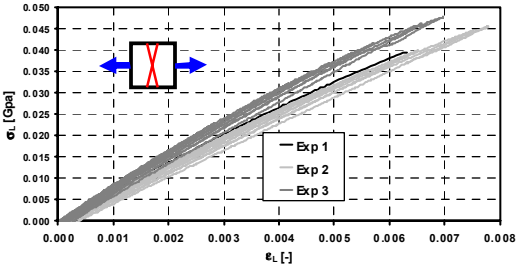

$[\pm 62]_{2s}$ cyclic tension

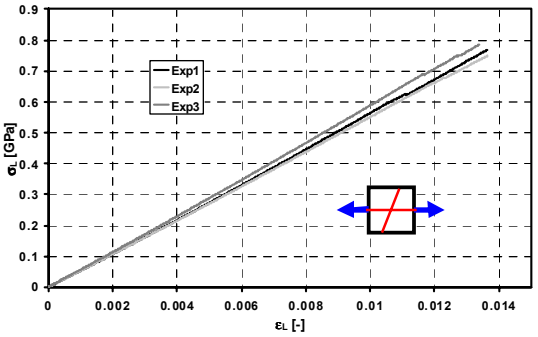

$[0/70]_{2s}$ tension

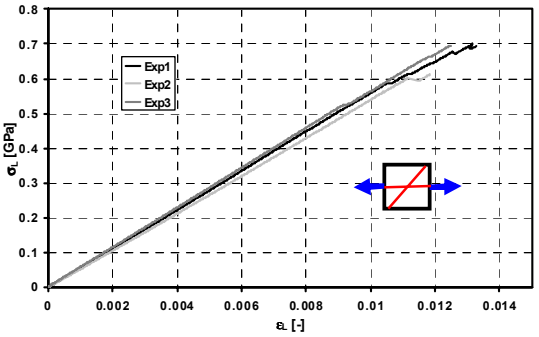

$[0/56]_{2s}$ tension

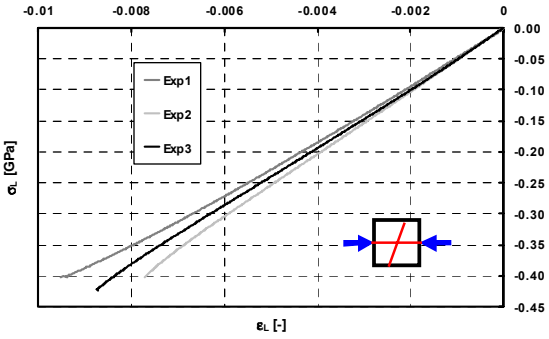

$[0/70]_{2s}$ compression

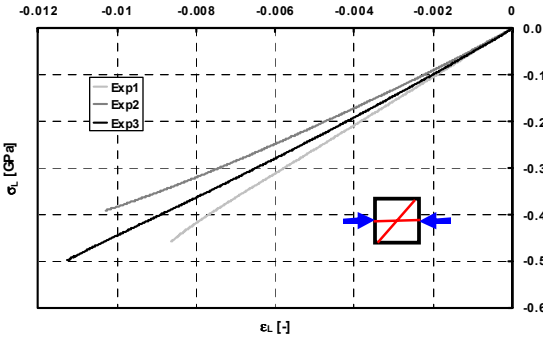

$[0/56]_{2s}$ compression

Table 1. Experimental longitudinal stress-strain curves for the pre-sheared NCF coupons.

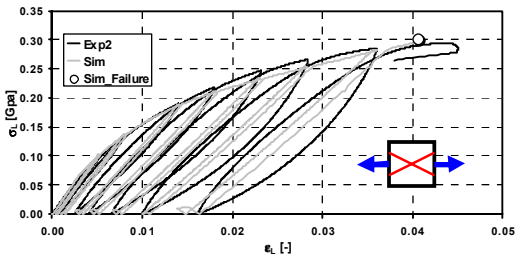

$[\pm 35]_{2s}$ cyclic tension

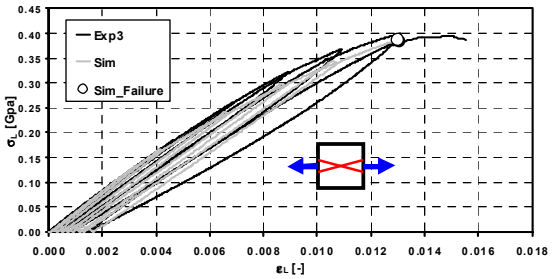

$[\pm 28]_{2s}$ cyclic tension

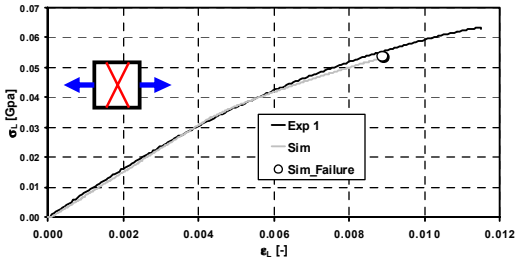

$[\pm 55]_{2s}$ cyclic tension

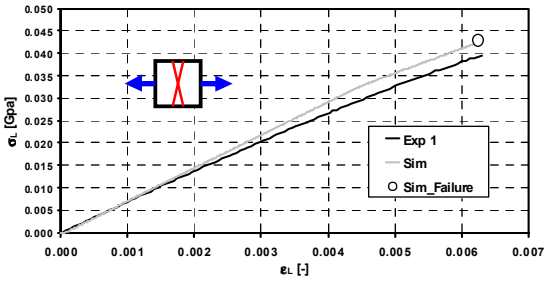

$[\pm 62]_{2s}$ cyclic tension

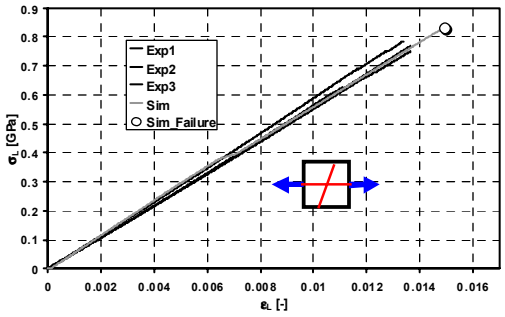

$[0/70]_{2s}$ tension

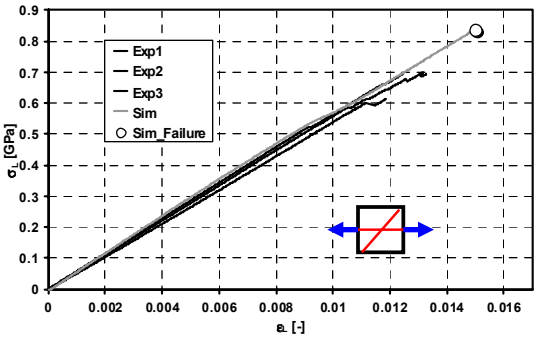

$[0/56]_{2s}$ tension

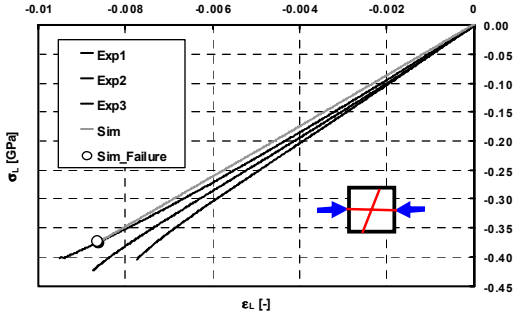

$[0/70]_{2s}$ compression

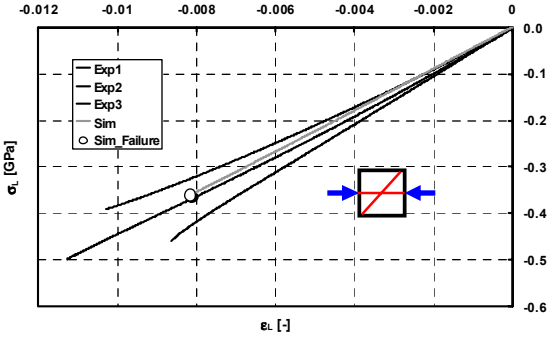

$[0/56]_{2s}$ compression

Table 2. Pre-sheared NCF coupons: Comparison of longitudinal stress-strain curves of experiments and simulations.

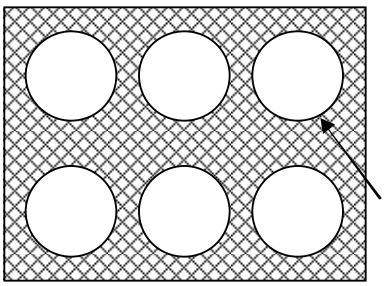

Disc extraction

Lay-up	Ø of punch [mm]	
	25	**50**
QI $[0/90/\pm45]_s$	3	3
$[\pm45]_{2s}$	2	3
$[\pm38/\pm52]_s$*	3	3
$[\pm35]_{2s}$*	2	2

*) Obtained from presheared ±45° NCF

Table 3. Test matrix for the transverse loaded composite discs using different lay-ups and punch diameters.

Lay -up	Small punch diameter (∅ = 25 mm)	Large punch diameter (∅ = 50 mm)
$[0/90/\pm45]_S$	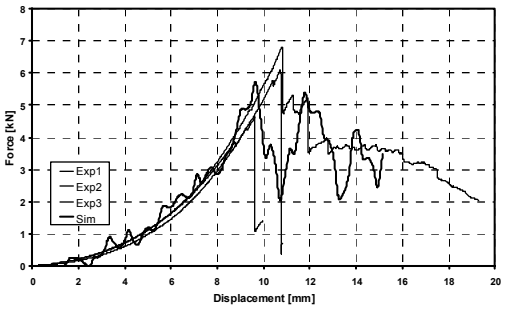	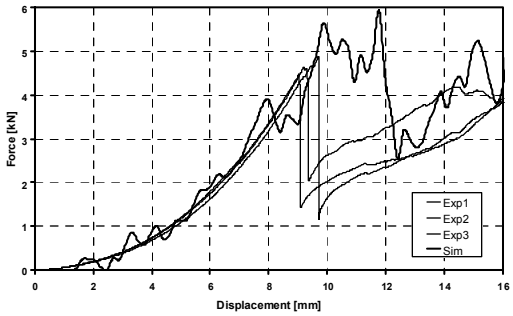
$[\pm45]_{2S}$	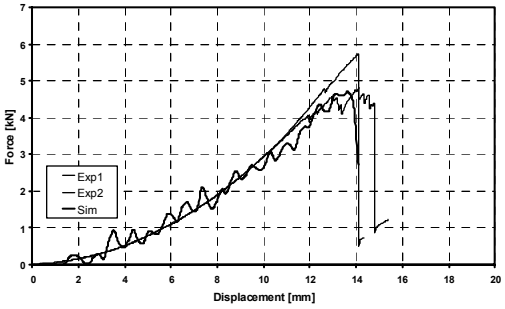	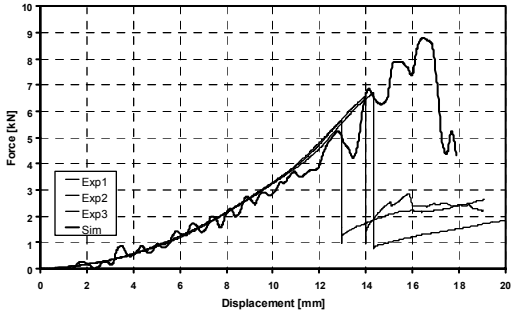
$[\pm35]_{2S}$	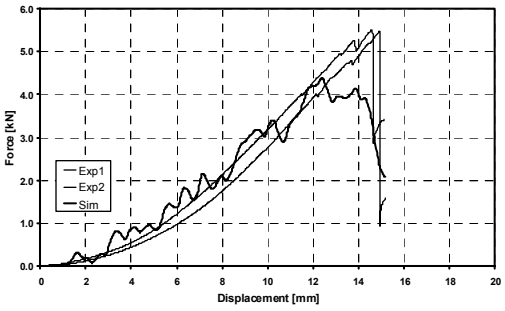	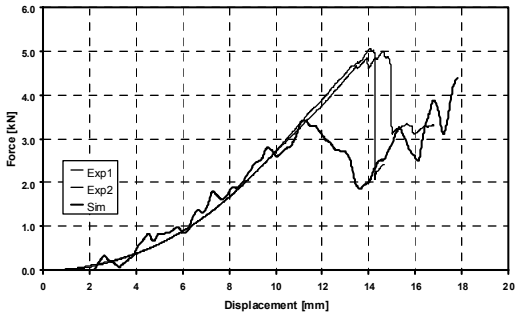
$[\pm38/\pm52]_S$	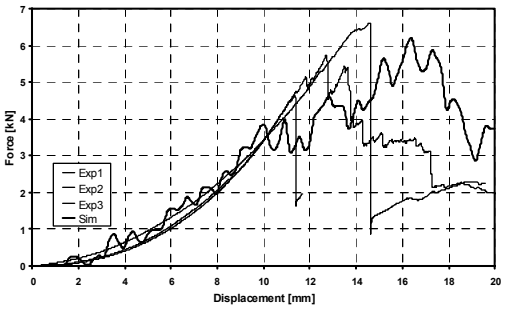	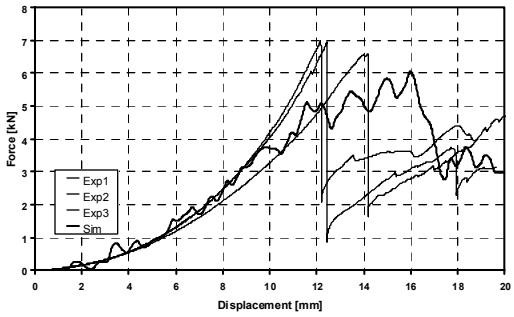

Table 4. Comparison of experimental and predicted force-displacement curves of transversely loaded NCF composite discs.

Lay-up	Small punch diameter (∅ = 25 mm)		Large punch diameter (∅ = 50 mm)	
	Fibre Failure	Matrix Failure	Fibre Failure	Matrix Failure
$[0/90/\pm45]_s$ 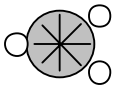	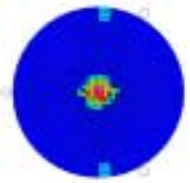	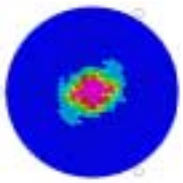	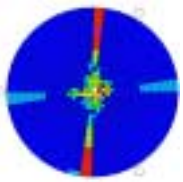	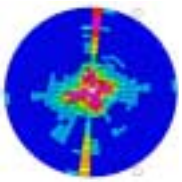
$[\pm45]_{2s}$ 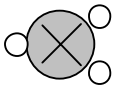	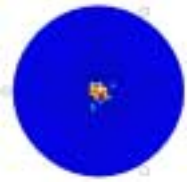	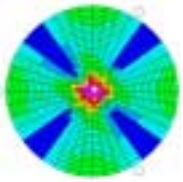	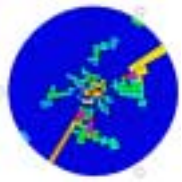	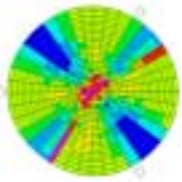
$[\pm35]_{2s}$ 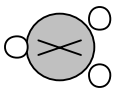	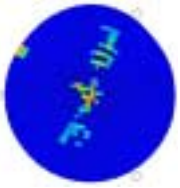	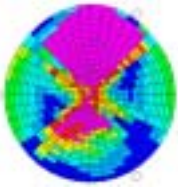		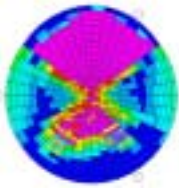
$[\pm38/\pm52]_s$ 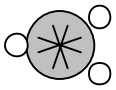	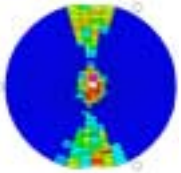	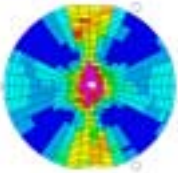	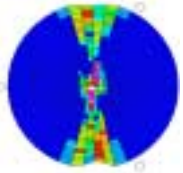	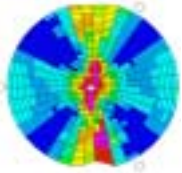

Highlighted regions indicate the average through-thickness damage state of fibre and matrix failure, respectively

Table 5. Contour plots of predicted fibre and matrix failure at the point of first structural failure for the composite discs using different punch diameters and composite lay-ups.

I. Appendix: Summary of Identified Material Parameters for Intra-laminar Ply Failure

	Notation	Symbol	Value
Elastic Properties	Fibre tension modulus	E_{11t}	*114 GPa*
	Fibre compression modulus	E_{11c}	*80 GPa*
	Matrix transverse modulus	E_{22}^{0}	*7.8 Gpa**
	Matrix shear modulus in 12-direction	G_{12}^{0}	*2.85 GPa*
	Matrix shear modulus in 23-direction	G_{23}^{0}	*2.50 Gpa**
	Poisson's ratio in 12-direction	υ_{12}^{0}	*0.32**
	Poisson's ratio in 21-direction	υ_{21}^{0}	*0.03**
	Fibre volume ratio	V_f	*0.48*
Plastic Properties	Matrix yield stress	R_0	*0.02 GPa*
	Matrix hardening coefficient	β	*0.67 GPa*
	Matrix hardening exponent	m	*0.52*
	Matrix anisotropy factor	a^2	*0.33*
Damage Properties	Initial shear damage threshold	$\overline{Y}_{12}^{0}$	*0.008 √GPa*
	Shear damage fitting parameter	$\overline{Y}_{12}^{fit}$	*0.035 √GPa*
	Damage state of saturation	d_{12}^{Sat}	*0.8*
	Initial transverse damage threshold	$\overline{Y}_{22}^{0}$	$\rightarrow\infty$
	Damage coupling factor	b	$\rightarrow 0$
Failure Properties	Maximum fibre tensile strain	$\varepsilon_{11,t}^{\max}$	*0.0155*
	Maximum fibre compression strain	$\varepsilon_{11,c}^{\max}$	*-0.01*
	Matrix transverse tensile strength	$R_{\perp}^{(+)}$	*0.050 GPa**
	Matrix transverse compression strength	$R_{\perp}^{(-)}$	*0.180 GPa**
	Matrix shear strength	$R_{\perp\parallel}$	*0.060 GPa*
	Failure envelope fitting parameter	$p_{\perp\parallel}^{(+)}$	*0.43*
	Failure envelope fitting parameter	$p_{\perp\parallel}^{(-)}$	*0.01*

*) Estimated values [7]

Table 6. Summary of identified material model parameters for biaxial carbon/epoxy NCF composite.

Paper: Composites Science and Technology

Modelling damage and failure in carbon/epoxy Non Crimp Fabric composites including effects of fabric pre-shear

L. Greve Volkswagen AG, Group Research, 38436 Wolfsburg, Germany

A. K. Pickett* School of Industrial and Manufacturing Science, Cranfield University, Bedford, MK43 0AL, United Kingdom

Response to reviewers

Reviewer #1: The paper presents a new numerical constitutive model for unidirectional laminae/non crimp fabric based on existing Ladeveze and Puck models. The model is implemented into explicit FE code and validated using an extensive range of experimental data. Results from the experimental programme include a range of fibre layups and pre-shear angles. The model is shown to capture the constitutive behaviour for transverse punch-loading very well.
The paper is well written and the results are presented clearly and thoughtfully -sufficient detail of the model is included.
This is a top quality paper and could be published as-is.
Minor recommendations would be to include a comment in the abstract related to the accuracy of the model, and to include more detail in the discussion of the results. There are a few typos which need correction and the references need to be reordered.

I have modified:

- *New sentence in the abstract stating accuracy of the model.*
- *A few typos (only 3) have been found and corrected.*
- *The references have been reordered and are now sequential*
- *I could not really see what to add in the discussion of results and feel that the important points are covered. Let me know if this is essential.*

Reviewer #2: The authors developed the modeling of intra-laminar failure prediction on non-crimp fabric composites which have gained great attention in automotive industry. In this manuscript, the authors pointed out that conventional Puck's failure modeling neglects inelastic material deformation and this model itself is not suitable to predict the failure of non-crimp fabric composites. Hence, the authors combined Puck's model with Ladeveze model which takes into account matrix plasticity and failure. Failure manner of non-crimp fabric composite disks subjected by the punch force were experimentally investigated and compared with finite element result input by the combined failure model. It was revealed that intra-laminar failure manner experimentally observed in composite disks well matched with the finite element result. It is considered that the failure modeling suggested by the authors is very useful to predict intra-laminar failure of non-crimp composites. Thereby, the publication of this manuscript for Composites Part A is highly recommended without revision.

- *No changes were requested.*

* Author for correspondence: Email a.k.pickett@cranfield.ac.uk

Modelling damage and failure in carbon/epoxy non-crimp fabric composites including effects of fabric pre-shear

Greve, L.

2006-11

Greve L, Pickett AK. (2006) Modelling damage and failure in carbon/epoxy non-crimp fabric composites including effects of fabric pre-shear. Composites Part A: Applied Science and Manufacturing, Volume 37, Issue 11, November 2006, pp. 1983-2001

http://hdl.handle.net/1826/1351